GLYCATION OF BETA AMYLOIDS AND THEIR CONTRIBUTION TO INSULIN RESISTANCE IN TYPE 2 DIABETES MELLITUS

by

Eric Kyunam Kim

A thesis submitted to Johns Hopkins University in conformity with the requirements for the

Degree of Master of Science in Engineering

Baltimore, Maryland

March 2020

Abstract

Type 2 Diabetes Mellitus (T2DM) is metabolic disorder that afflicts 200,000 Americans per year and a total of 463 million people globally. Due to significant dietary changes that increase intake of fats and sugars, 9.5% of Americans over 18 years old begin to develop pre-diabetes old and left untreated should expect to develop T2DM within 5 years. Although researchers have been able to link diet, genetic factors and epigenetic factors to T2DM, the mechanism through which Type 2 Diabetes develops remains elusive. Diabetic patients experience a wide range of symptoms, the most significant of which are impaired insulin action, hyperlipidemia, and chronic inflammation. Recently researchers have observed that beta amyloid accumulation can cause insulin resistance both directly and indirectly. Beta amyloids can bind to cell surface and cause chronic inflammation by over-stimulating the JAK/STAT pathway as well as cause free fatty acid (FFA) accumulation within cells through CD36 activation caused by Ca2+ influx. Glycation, the non-enzymatic addition of glucose molecules to beta amyloids, also can contribute significantly to the accumulation of beta amyloids in the body. Beta amyloids in high glucose environments appear to exhibit reduced clearance for in vivo models similar to those of glycosylated beta amyloids due to London and Sweden mutation exhibiting patients. This information suggests that glycated beta amyloids show decreased elimination compared to non-glycated beta amyloids. In this paper, we explore the potential accumulation of beta amyloids and glycated beta amyloids through a multi-compartment model sensitivity analysis that adjusts the glycation rate constant and perfusion of glucose between the intestines and visceral adipose tissue. From our results we conclude that the glycation reaction rate of beta amyloids has a greater variability on the overall accumulation of glycated beta amyloids than the concentration of glucose in the organ compartments. This variability is dependent on whether the

patient consumes high glycemic index (GI) meals or low GI meals. However, it is unknown if such small changes to blood volume glucose concentrations will result in insulin resistance potential. Future development of the model should implement the influx of beta amyloids into tissue volume compartments via primarily receptors for advanced glycation end products (RAGEs).

Contents

Abbreviations and Notations

AD – Alzheimer's disease: A neurodegenerative disease that worsens cognitive and physical functions over time. [18]

AGEs – Advanced Glycation End Products: Highly processed glycated molecules which functions are inhibited and can accumulate in the body. (Most tissues and blood) [37]

APP – Amyloid Precursor Protein: A membrane protein which when cleaved creates beta amyloid proteins. (Most Tissues) [29]

CD36 – Cluster of Differentiation 36: A membrane protein which facilitates the intracellular influx of free fatty acids from the bloodstream. (Primarily adipocytes, hepatocytes, and myocytes) [11]

C-Jun – C-Jun: A downstream protein which drives the pro-inflammatory process within a cell. (Most cells) [14]

EGFR – Epidermal Growth Factor Receptor: A transmembrane protein which binds to epidermal growth factor family proteins. (Most cells) [21]

FFAs – Free Fatty Acids: Non-esterified fatty acids that are bound to a transport protein which circulate in the plasma. (Bloodstream) [9]

GI – Glycemic Index: A score associated with food which signifies the potential rise of blood glucose levels two hours after eating a meal.

GLUT4 – Glucose Transporter Type 4: An insulin-regulated protein which facilitates the absorption of glucose into a cell. (Primarily adipocytes, hepatocytes, and myocytes) [2]

IKK – IκB Kinase: An enzyme complex involved in the activation of nf-κB transcription factors for pro-inflammatory responses. (Most cells) [14]

IRS – Insulin Receptor Substrate: An insulin-dependent signaling protein which activates the insulin action within a cell. (Primarily adipocytes, hepatocytes, and myocytes) [2]

JAK – Janus Kinase: A family of pro-inflammatory signaling proteins in the JAK/STAT pathway. (Most Cells) [13]

JNK – c-Jun N-terminal Kinases: A pro-inflammatory signaling protein in the MAPK pathway. (Most Cells) [14]

KO – Knock-Out: A technique which inactivates genetic expression of a specific gene. [12]

krxn – Glycation reaction rate: The glycation reaction rate of a glucose molecule and a non-glycated beta amyloid protein.

MAPK – Mitogen-Activated Protein Kinase: A pro-inflammatory signaling pathway that involve responses of inflammatory cytokines. (Most Cells) [13]

NEP – Neprilysin: A zinc-dependent metalloprotease which can degrade many proteins including beta amyloid peptides. (Most tissue and blood) [33]

nf-κB – nuclear factor kappa-light-chain-enhancer of activated B cells: A protein complex which controls cellular functions including cytokine expression for inflammation. (Most Cells) [13]

PI3K - Phosphoinositide 3-kinase: A family of enzymes responsible for activating PIP2 to PIP3 for many cell functions including insulin signaling. (Most Cells) [2]

PIP2 - Phosphatidylinositol 4,5-biphsophate: Dephosphorylated phospholipid of PIP3 which is phosphorylated by PI3K. (Most Cells) [2]

PIP3 - Phosphatidylinositol 3,4,5-triphsophate: Phosphorylated phospholipid which activates downstream proteins such as protein kinase B. (Most Cells) [2]

PKB – Protein Kinase B: A protein which when phosphorylated is responsible for many cell functions including insulin signaling. (Most Cells) [2]

PKC - A protein which activates MAPK pro-inflammatory pathway. (Most Cells) [14]

Q – Perfusion Flow Rate: Perfusion of glucose from the intestines to the visceral adipose tissue.

RAGEs – Receptors for AGEs: Receptors that facilitate absorption of advanced glycated end products. (Most Cells) [44]

SOCS - Suppressors of Cytokine Signaling: Anti-inflammatory proteins transcribed by STATs which inactivate JAK proteins in inflammatory process. (Most Cells) [13]

STAT - Signal Transducer and Activator of Transcription: Transcription factor proteins activated by janus kinase proteins to being production of pro-inflammatory cytokines and SOCSs. (Most Cells) [13]

T2DM – Type 2 Diabetes Mellitus: A glucose metabolic disease which affects the cell's ability to properly respond to insulin. [1]

VAT – Visceral Adipose Tissue: Adipose tissue that directly surrounds major organs in the abdominal cavity. (Abdominal cavity)

Acknowledgements

I would like to thank Dr. Donohue for giving me this opportunity to work on my Master's thesis with him, as well as his guidance throughout the process.

I would also like to thank Dr. Betenbaugh for spending his time to attend my thesis presentation.

Finally, I thank my co-captain in my everything-ship for her unwavering support through the rogue waves.

List of Tables

List of Figures

Introduction

Type 2 Diabetes Mellitus (T2DM) is a metabolic disease that affects glucose homeostasis [1]. Approximately 200,000 Americans per year are diagnosed with T2DM and a total of 463 million people globally are affected by several health complications associated with prolonged presence of high glucose levels including: neuropathy, kidney failure, and increased risk of heart attacks and strokes [1]. Significant T2DM symptoms include impaired insulin action, hyperglycemia, hyperlipidemia, hyperinsulinemia, and chronic inflammation [1]. Although researchers have tied this disease to diet and epigenetic factors, the primary cellular pathology remains elusive. Currently, researchers have proposed different mechanisms of action that directly affect insulin action: lipid accumulation in tissue, lipopolysaccharides, pro-inflammatory cytokines that cause chronic inflammation, and hyperinsulinemia. In order to ascertain the T2DM mechanism of action, we must understand insulin action within the cells, associated organs, glucose metabolism, and chronic inflammation.

Because prolonged high concentrations of glucose are neurotoxic, insulin exerts different effects on skeletal muscle, liver, and adipose tissue in order to control significant increases of blood glucose concentrations. The pancreas secretes insulin once it senses glucose concentrations significantly above a certain threshold [2]. Once secreted, insulin binds to specific insulin receptors in the organs to start an intracellular process involving phosphoinositide 3-kinase (PI3K) and protein kinase B (PKB), also known as Akt, to translocate the vesicles containing GLUT4 transporter to the cell membrane as shown by *Figure 1* [3].

Figure 1 [3]: Basic Insulin Action on Cell to Translocate GLUT4 to Cell Membrane

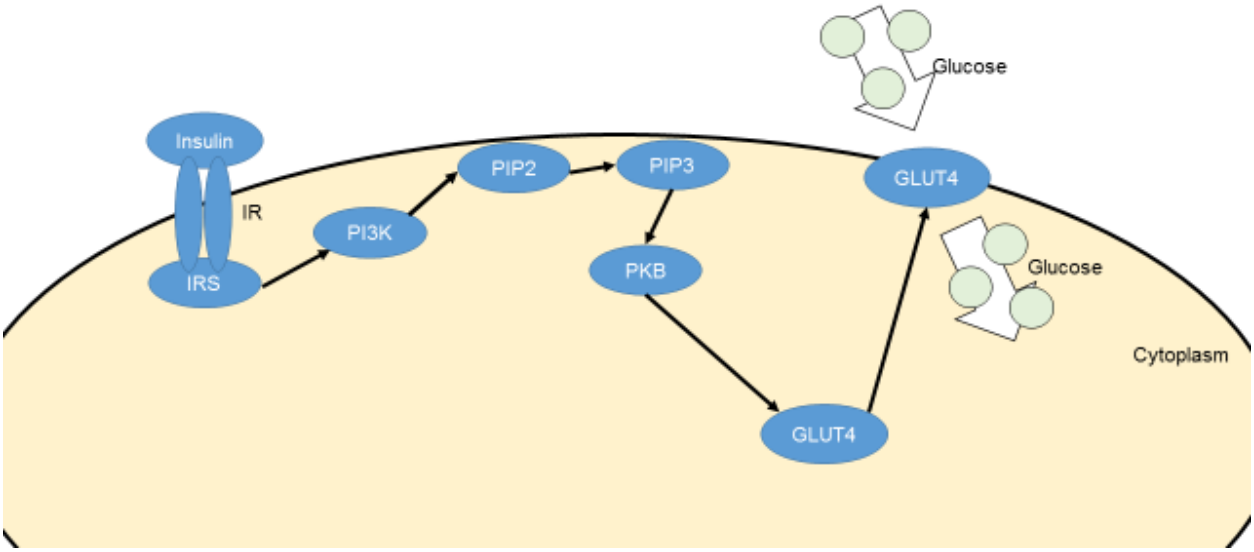

This process involves the activation of insulin receptor substrate (IRS) once the insulin binds to the insulin receptor [2]. The IRS then activates PI3K to convert phosphatidylinositol 4,5-biphsophate (PIP)2 to PIP3 [2]. PIP3 then activates PKB which then facilitates the translocation of glucose transporter type 4 (GLUT4) to the cell membrane [2].

Not only does insulin initiate GLUT4 translocation to the cell membrane, but it also affects different metabolic processes dependent on the organ [4]. Insulin overrides normal metabolic processes by inhibiting lipid metabolism in skeletal muscle, adipose tissue, and the liver to return glucose levels to their baseline levels [2]. Most importantly, insulin inhibits glycogenolysis the cleavage of glycogen --a polysaccharide of glucose -- stored in the liver and skeletal muscle functions to decrease glucose levels, to focus on glycolysis from absorbed glucose [4]. Insulin also stimulates the liver and skeletal muscle to begin glycogenesis in an effort to store glucose as glycogen stores inside those organs [4]. When insulin is high, it also slows lipolysis of triglycerides into free fatty acids and therefore reduces their release into the

plasma by adipose tissue. The adipose tissue also converts absorbed glucose into glycerol [4]. After the lowering of glucose in the plasma by these responses to insulin, the pancreas begins to release glucagon to help maintain g exerts these effects in tandem with the glucagon hormone to assist in maintaining glucose homeostasis after there is no longer glucose intake into the body [5]. The pancreas secretes glucagon in response to the blood glucose levels dipping below the baseline levels [5]. Glucagon binds to glucagon receptors in the liver and skeletal muscle to begin glycogenolysis [5]. Glycogen phosphorylase cleaves a glucose-1-phosphate from the terminus of glycogen molecules until all the glucose stored in glycogen [5]. After the liver and skeletal muscle deplete their glycogen stores, glucagon promotes gluconeogenesis which generates glucose from non-carbohydrate sources including lipids, glycerol, and proteins to maintain basal blood glucose levels [5]. These processes can be seen in *Figure 2*.

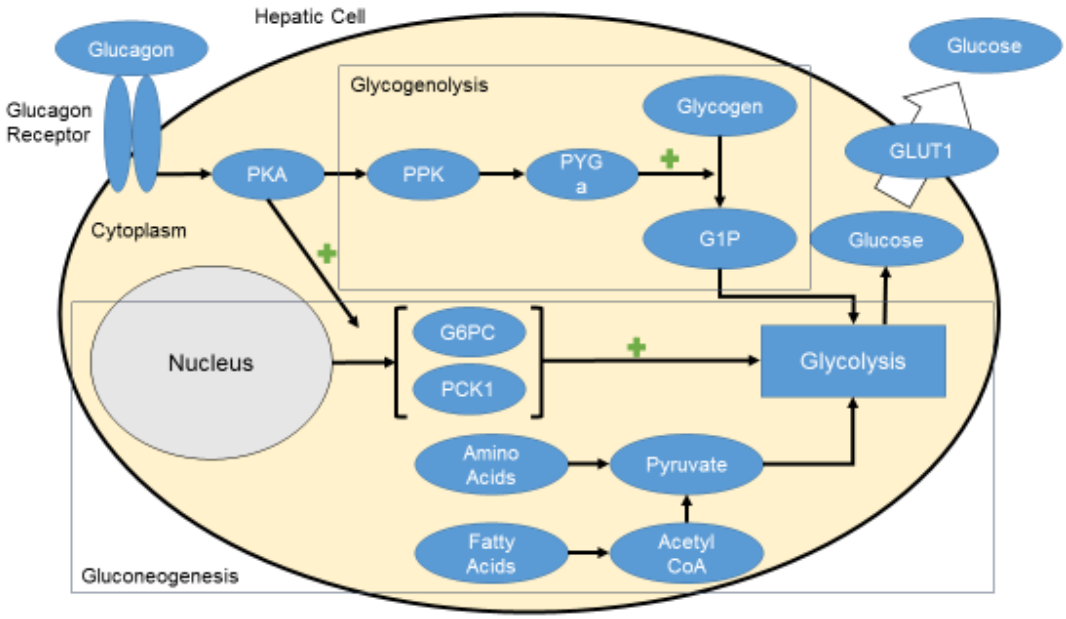

Figure 2 [6]: Glucagon Effect on Hepatic Cell. In gluconeogenesis, PKA begins the transcription of G6PC and PCK1 in the nucleus, which then promote the conversion of non-glycogen sources such as amino and fatty acids into glucose [6]. The plus marks indicate an upregulation of processes [6]. The large arrow indicates the transport of glucose through the GLUT1 membrane protein.

Insulin resistance results in a decrease of GLUT4 to the cell membranes and thereby affects the ability of the liver, adipose tissue, and skeletal muscles take glucose out of the plasma to maintain glucose homeostasis [5]. Without proper insulin action in the body, important organs involved in glucose homeostasis not only fail to absorb glucose with GLUT4, but also fail to switch metabolism targets: 1) failed inhibition of glucagon secretion causes the liver to continue to secrete glucose into the bloodstream, 2) the skeletal muscle continues to preferentially metabolize fats instead of glucose, and 3) adipose tissue continues to secrete fat into the bloodstream [7]. As a consequence, T2DM patients have an inability to preferentially metabolize glucose and begin to experience not only higher normal glucose levels, but also prolonged exposure to those heightened glucose levels [1]. To find potential mechanisms of actions that result in T2DM, researchers have explored the comorbidity of T2DM and obesity, and they discovered potential links between fat accumulation and insulin resistance in T2DM patients [8].

FATTY ACID ACCUMULATION

Along with impaired insulin action, T2DM patients experience hyperlipidemia and increased lipid content in certain organs [8]. As mentioned earlier, insulin resistance causes the adipose tissue to continue to secrete free fatty acids (FFAs) into the bloodstream, in spite of insulin binding to its receptors [9]. Concurrently, the insulin resistant liver and skeletal muscle continue to absorb FFAs from the bloodstream, and they tend to accumulate FFAs due to an impaired metabolism of FFAs [10]. The impaired metabolism of FFAs may be due to mitochondrial defects within affected cells since researchers observed a lack of FFA oxidation in insulin resistant skeletal muscle [10]. The liver and skeletal muscle absorb FFAs with the translocation of the CD36 membrane protein [11]. CD36 translocation to the cell membrane requires an influx of Ca2+ ions which are controlled by ion transporters [11]. Therefore an

abnormal influx of Ca2+ ions into cells can cause upregulated translocation of CD36 to the cell membrane, leading to FFA accumulation within upregulated CD36 protein-specific tissue. Accumulation of FFAs can increase the concentration of harmful intracellular FFA metabolites, such as ceramide and palmitic acid, which can cause deleterious effects including impaired insulin action through inhibition of Akt processes [10]. Researchers have experimented with insulin sensitivity in CD36 knock-out (CD36KO) mice [12]. When compared to their diabetic controls, CD36KO mice experienced increased insulin sensitivity [12]. However, researchers were not able to completely cure diabetic rats by inhibiting CD36 production. This suggests that there may be additional cellular processes affecting cellular insulin action. To this end, researchers have also observed FFA metabolites activating cellular pro-inflammatory processes through binding to inflammatory receptors, potentially overstimulating pro-inflammatory processes that lead to the accumulation of intracellular pro-inflammatory cytokines [10].

INFLAMMATION

The inflammation cellular process involves the presence of pro-inflammatory and anti-inflammatory cytokines [13]. The balance of each interaction results in an acute activation of an inflammatory state of cells that should resolve over time [13]. An imbalance in these interactions may lead to a prolonged inflammatory environment which can cause a variety of chronic illnesses and diseases such as rheumatoid arthritis and lupus nephritis [13]. While the inflammation process can span in various tissues and organ systems, we will focus on the inflammation that occurs on a single cell [13].

Activated macrophages are the primary producers of inflammatory cytokines which up-regulate the inflammatory process [13]. Up-regulation results in an increase in cytokine expression within cells and a cascade of pro-inflammatory effects through three primary

pathways: nf-kB pathway, MAPK pathway, and the JAK/STAT pathway [13]. The nf-kB pathway controls the pro-inflammatory cytokine expression as well as cell recruitment that contribute to the pro-inflammatory response [13]. The MAPK pathway includes a family of serine/threonine protein kinases that activate the cellular responses of inflammatory cytokines and other proteins [13]. Through the activation of the MAPK process, p38 transcription factors phosphorylate to initiate transcription factors in the cell nucleus, thus activating the inflammatory response [13]. The JAK/STAT pathway is unique to the previous processes as extracellular factors such as interleukin-6 (IL-6) directly affect gene expression [13]. JAKs associated with their respective receptors phosphorylate each other to activate their respective STATs via phosphorylation [13]. STATs then dimerize before translocating to the nucleus, where they bind to gene promoter regions to upregulate transcription of inflammatory genes [13]. The inflammatory cytokines expressed in the nucleus exit the cell and bind to other cell surface receptors [13]. From these inflammatory pathways, researchers have observed how inflammation can directly cause insulin resistance through intracellular insulin signaling mechanisms [14].

Researchers have been able to map certain inflammatory pathway products that have an effect on insulin resistance. Such products have been shown to inhibit the IRS protein directly [14]. Upstream products include the PKC, JNK, and IKK proteins which are activated by several substrate receptors including the LTB4, ANG II, FFAs, TNF-α, and IL-1β [14]. Researchers believe these proteins may cause insulin resistance by presently unknown processes [14]. In addition to the PKC, JNK, and IKK proteins, downstream inflammatory substrates such as the C-Jun and nf-κB induce production of inflammatory molecules and inflammasomes [14]. Inflammasomes and inflammatory molecules induce further activation of inflammatory receptors

once secreted outside the cell [14]. Furthermore, inflammatory molecules can also directly inhibit IRS function [14]. These pathways are shown in *Figure 3*.

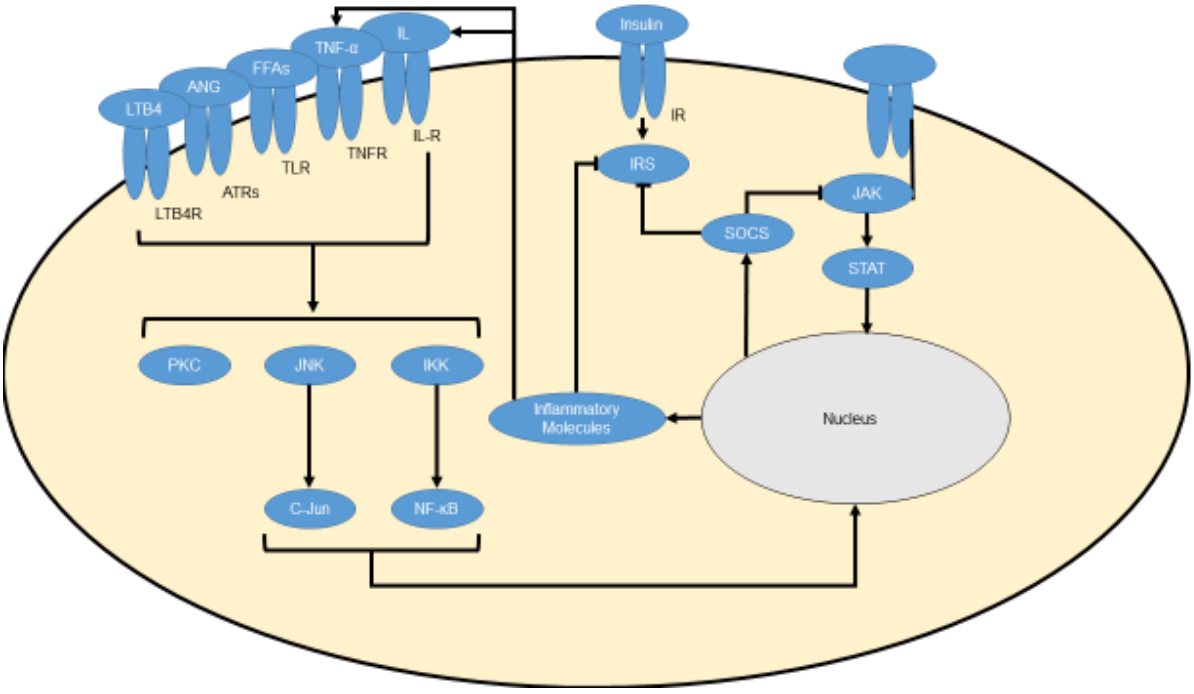

Figure 3 [14]: Inflammatory Effect on Cellular Insulin Action. Cellular pathways for inflammation to affect insulin response in a skeletal muscle cell.

The activation of the JAK/STAT pathway also results in the expression of anti-inflammatory cytokines suppressor of cytokine signaling (SOCSs) which bind to JAK to suppress its activation [13]. Researchers have proposed that the JAK/STAT pathway, through the suppression of SOCSs, contribute to let pro-inflammatory processes run rampant [13]. Researchers have experimented with SOCS KO mice, discovering that such mice experienced increased insulin resistance when compared to control mice, suggesting that a rampant inflammatory process through the JAK/STAT pathway may have a significant contribution to insulin resistance [15]. Furthermore, researchers have observed that JAK/STAT KO diabetic mice demonstrate increased insulin sensitivity compared to control diabetic mice [16]. What is most interesting is that one study measured insulin sensitivity between JAK/STAT KO mice in

different organs [17]. They observed that liver-specific JAK/STAT and adipose-specific JAK/STAT KO mice had improved insulin sensitivity compared to diabetic mice. However, mice with both liver- and adipose-specific JAK/STAT KO retained insulin sensitivity comparable to healthy control mice despite liver steatosis, which is normally associated with insulin insensitivity [17]. These results suggest that the interaction between the liver and adipose tissue has a significant role in the development of insulin resistance. In addition, it is possible to assume that the JAK/STAT pathway has a significant contribution to the development of insulin resistance in the pathology of T2DM. When we consider both the symptomatology of chronic inflammation and fat accumulation within tissue, we find that beta amyloids can cause all these symptoms in T2DM patients.

APPs AND BETA AMYLOIDS

Beta amyloids, or amyloid betas, are processed peptides products of length 39-43 amino acids [18]. Extracellular accumulation of beta amyloids have been implicated in Alzheimer's disease and more recently T2DM [18]. Beta amyloids can exert insulin insensitivity through direct and indirect processes. The membrane-binding of beta amyloids can cause depolarization of cell membranes, which may in turn cause an overstimulation of CD36 translocation to the cell membrane [19]. This increases the FFA influx and can result in accumulation of FFA and harmful FFA metabolites, thereby decreasing insulin activity [10]. Furthermore, beta amyloids overstimulate the JAK/STAT pathway, causing chronic inflammation in the cells [20]. Through the JAK/STAT pathway, beta amyloids lead to an increase in the expression of pro-inflammatory cytokines [20]. In normal cellular inflammatory processes, the nucleus would begin to produce SOCS proteins that directly inhibit JAK activity [21]. However, beta amyloids can stimulate the epidermal growth factor receptor (EGFR) which can inactivate the SOCSs, hindering the cell's

ability to shut down its own anti-inflammatory pathway [21]. Another potential outcome of the inactivation of SOCS can lead to intracellular SOCS accumulation [22]. The cell may continue to upregulate SOCSs in a futile attempt to suppress the JAK/STAT inflammatory pathway, leading to an accumulation of intracellular SOCSs [22]. These SOCSs can negatively affect insulin action by the deactivating IRS proteins through inhibition of tyrosine phosphorylation [22]. In addition, SOCSs can also increase production of ceramide which inhibits PI3K and Akt proteins [23][24]. Not only are PI3K and Akt integral to the final activation of GLUT4 translocation, these proteins also mediate several other processes, such as cell migration and recruitment [25], which researchers have observed to be hindered in T2DM and other chronic inflammatory-disease patients [26].

As people age, they begin to experience the effects of beta amyloid accumulation in tissue and blood [27]. However, significant accumulation of beta amyloids appears to not happen in all aging people sufficiently to cause neurodegenerative diseases. This suggests that there are other parameters that cause either the upregulated expression of beta amyloids or the decrease of beta amyloid clearance or both [28]. Chen has suggested that particulate air pollution may be involved in the upregulation of misfolded beta amyloids that cause both Alzheimer's and Parkinson's diseases [28].

Beta amyloids are byproducts of amyloid precursor proteins (APPs) processing. APPs are a class of transmembrane proteins that undergo post-translational modification that result in proteolytic cleavage to peptide fragments and other products [29]. Through secretase (beta and gamma) cleavage of APPs, beta amyloids are generated at varying lengths [29]. Although researchers have investigated the inhibition of gamma secretase as a means of preventing beta amyloid production, there appears to be several underlying processes that also produce beta amyloids

from APPs, which render the inhibition of gamma secretase paradoxically ineffective [29]. Researchers investigating Alzheimer's Disease (AD) have narrowed down beta amyloids 1-40 and 1-42, marked by the length of their peptide chain, as the most harmful beta amyloids [30]. These beta amyloid species have been linked to T2DM with a potential shared pathology with AD [31]. Typically proteolytic degradation of beta amyloids account for the majority of its clearance [32]. While there are many classes of proteins which can degrade beta amyloids, we chose to focus on neprilysin (NEP) due to the abundance of literature that characterizes it.

NEP is a zinc-metalloprotease which faces the plasma side of the cell. It primarily degrades peptides of 40 to 50 residue lengths, and NEP has the ability to degrade more toxic beta amyloid oligomers as well as monomers [33]. Researchers have discovered that NEP KO mice experienced increased levels of beta amyloids in the brain [33]. Furthermore, researchers have transferred the NEP gene into AD transgenic mice and discovered a reversal of amyloid-like pathology and improvements in animal behaviors [33]. Baseline NEP tissue concentrations in people appears to decrease with age, and researchers suggest that this reduction may lead to increased risk of beta amyloid aggregation in cerebral amyloid angiopathy of AD patients [33]. Other notable protein degradation mechanisms include other classes of zinc-metalloproteases other than NEP, NEP-like proteases, endothelin-converting enzymes, angiotensin-converting enzyme, matrix-metalloproteases, insulin-degrading enzymes, serine proteases, and many more [34]. However, it is unknown the extent to which decreased levels of degradation proteins contribute to the pathogenesis of beta amyloid accumulation. An abnormal clearance of beta amyloids due to protein modification by glycation, non-enzymatic glucose addition, may also contribute more to beta amyloid accumulation. Paired with hyperglycemia and impaired glucose

clearance, glycation may occur more often in individuals at-risk for developing diabetes, compared to healthy controls.

GLYCATION OF BETA AMYLOIDS

Glycation typically involves a protein or a lipid, covalently binding to a glucose, fructose, or glucose/fructose derivatives in a multistep reaction process [35].

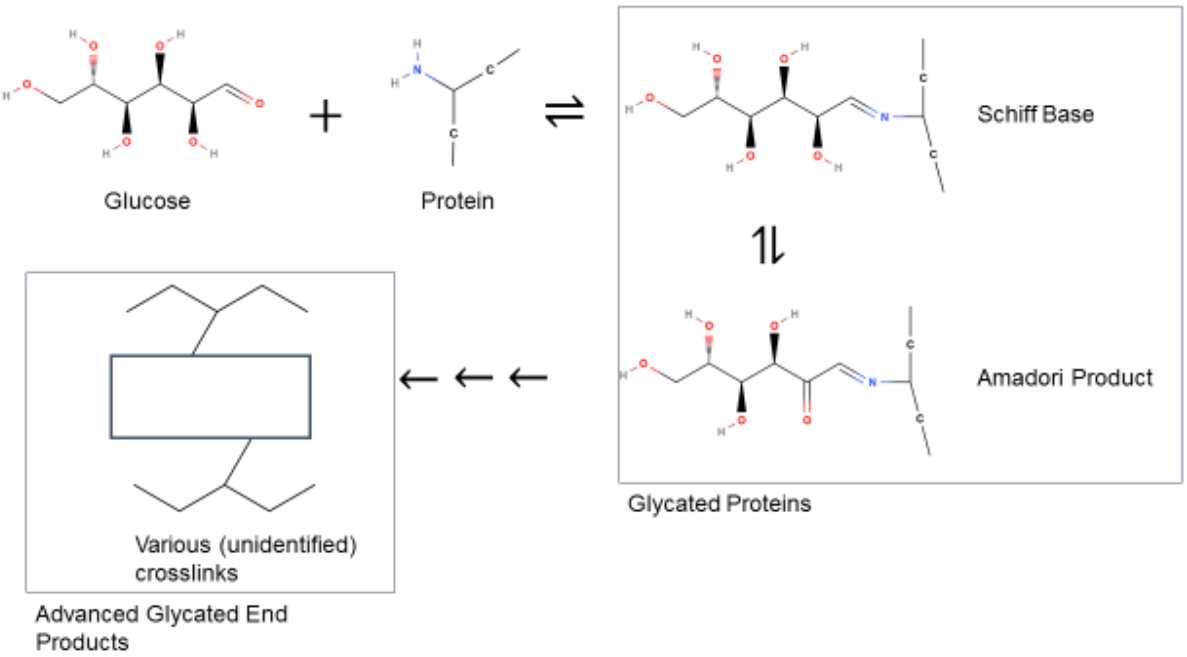

Figure 4[36]: Glycation Reaction Mechanism to Form Advanced Glycated End Products.

Glycation begins with a sugar molecule non-enzymatically binding to a free amino acid, typically a lysine or arginine residue, to form a Schiff base [37]. This Schiff base undergoes reversible rearrangement (Amadori Rearrangement) to form a more stable Amadori product [37]. An Amadori product can undergo further stabilization through a formation of an adduct or protein crosslink which becomes practically irreversible [37]. Further environmental interactions, typically oxidation, converts the Amadori product to form a variety of advanced glycation end products (AGEs) [37]. Researchers have found that AGEs are responsible for a variety of chronic conditions including inflammation [37]. AGEs tend to accumulate over time since its

modifications decrease clearance rates in the body [37]. The rate at which beta amyloids are glycated is dependent on the type of sugar binding to them [37]. Researchers have observed that fructose has a glycation rate tenfold to that of glucose [38]. While epigenetic predisposition to T2DM is important towards the pathogenesis of T2DM, the prolonged presence of glucose due to high-glucose diets may potentially cause increased glycation within patients [1][39].

Researchers have found that in high glucose environments, beta amyloids experience a decrease in clearance similar to that of beta amyloids in patients with London and Sweden genetic disorders which result in the N-linked glycosylation of beta amyloids [39]. More specifically, the species of beta amyloids in question are 1-40 and 1-42. Although researchers have linked beta amyloids 1-42 to most physiological problems associated with Alzheimer's, this protein has a tendency to aggregate into fibrils which accumulate mostly in the brain [40]. However, glycation of beta amyloids 1-42 has been proven to decrease the concentration of beta amyloid 1-42 fibrils, which suggests that glycated beta amyloid 1-42 exists as a peptide rather than a fibril [41]. This corroborates with other studies investigating beta amyloid 1-40 and 1-42 plasma concentrations between healthy and T2DM patients. Researchers observed a total decrease of plasma beta amyloids in T2DM patients compared to controls, but an increase in the ratio of plasma 1-42 to 1-40 beta amyloids compared to controls [42]. Although the plasma concentration of beta amyloids decreases in T2DM patients, their tissue beta amyloid concentration is significantly greater than those of a control patient [43]. This suggests that tissues are absorbing beta amyloids at a greater rate likely due to the prolonged presence of beta amyloids potentially due to glycation in T2DM patients. Receptors of AGEs (RAGEs) bind to glycated beta amyloids from the bloodstream and deposit bound proteins into organ tissue [44].

RAGEs appear to bind to beta amyloid peptides more than their oligomer counterparts as well as recruit more RAGEs to the apical blood vessel membrane [44].

Therefore, it may be important to study the accumulation of beta amyloids, glycated and non-glycated species, to ascertain if its significant accumulation can be the primary cause of insulin resistance in T2DM patients. So far, we observed that FFAs can exert insulin resistance by affecting both upstream and downstream insulin processes. In addition, we observed that the JAK/STAT pathway can not only exacerbate FFA-related insulin resistance but also inhibit upstream insulin processes. A potential unifying mediator of these symptoms may be related to beta amyloids. Beta amyloids can exert chronic inflammation as well as lipid accumulation in cells. We attempted to study the potential effects of diet on the accumulation of beta amyloids, glycated and non-glycated species, by creating a multi-compartment model using MATLAB.

MULTI-COMPARTMENT MODELING

Using a system of ordinary differential equations researchers can create multi-compartment models to predict pharmacokinetic concentration profiles of several substances. Along with the basic assumptions used for multi-compartment modeling, we used additional assumptions to simplify the complex systems of glucose homeostasis and beta amyloid production. The differential equations for this model are listed in Appendix 1. The parameters for the rate constants are given in Appendix 2.

MODELING OF GLUCOSE HOMEOSTASIS

Our purpose in creating this multi-compartment model is to observe how diet can affect the accumulation of beta amyloid species in specific organs. We simulated glucose homeostasis

in our multi-compartment model to be able to simulate long term effects of a high/low glucose diet and compare the differences between each respective beta amyloid species accumulation.

Our glucose homeostasis model only includes the primary organs involved in glucose absorption and insulin action as compartments: the blood in the central compartment (i.e. the circulatory system), intestines, visceral adipose tissue (VAT), pancreas, liver, and skeletal muscle of a 70 kg male. The volume of the compartments represent the blood volumes inside each compartment, and the blood flow rates represent the average blood flow rates from the heart to each specific organ. We set the baseline blood glucose concentration at ~85 mg/dL. We assumed that the brain consumes glucose from the circulatory system at a constant rate. Furthermore, we added a glucose dose representing a meal that has a flow-rate from the food to the intestines. The glucose dose is representative of the typical glucose mass in a dinnertime meal. Studying peritoneal absorption of nutrients as a method of dialysis, researchers have observed a potential for the perfusion of nutrients from the intestines to the surrounding cells [45]. We represented this perfusion as a flow from the intestinal compartment to the VAT compartment. The table containing the values of the volumes and blood flows between each compartment used are listed in Appendix 2. The blood flows between each compartment are shown in *Figure 5*.

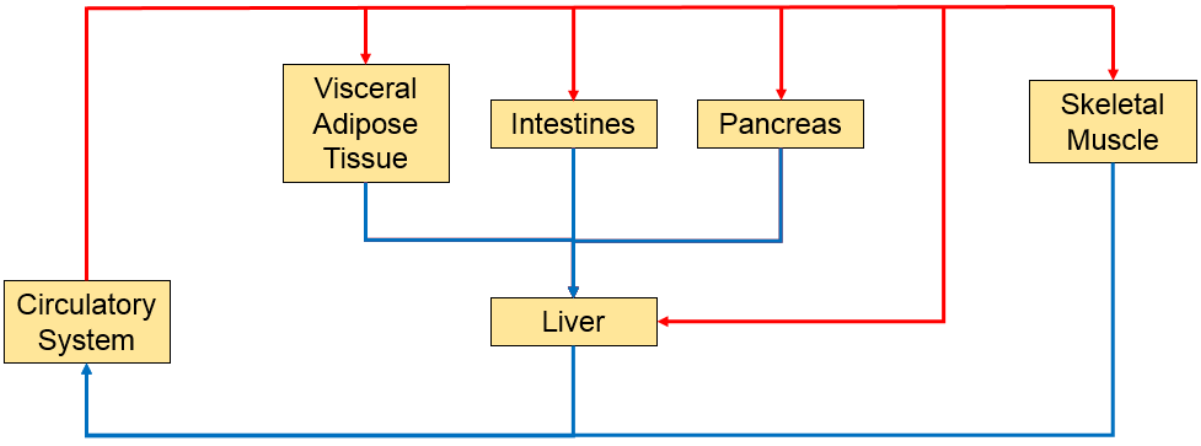

Figure 5: Multi-Compartment Model. The blood flows begin from the circulatory system and flow to each organ listed above. The visceral adipose tissue, intestines, and pancreas compartment have an exit flow directly to the liver representing the portal vein. The portal vein directly flows into the circulatory system.

We first modeled the glucose, glucagon, and insulin concentration profiles after a single meal. Glucagon and insulin follow the same compartmental model as that of glucose. The pancreas appropriately secretes each of these hormones by detecting differences in glucose concentration within its compartment [2]. At homeostasis, the pancreas secretes an appropriate amount of glucagon and insulin to maintain their baseline hormone concentration in the model. At fasting, the pancreas will secrete its baseline glucagon rate to prevent hypoglycemia in the model, and insulin will inhibit the secretion of glucagon when the blood glucose concentration rises above 110 mg/dL. We use data from a glucose meal study between pre- and post-gastric bypass patients to match the parameters observed in patients with a high glucose meal [46].

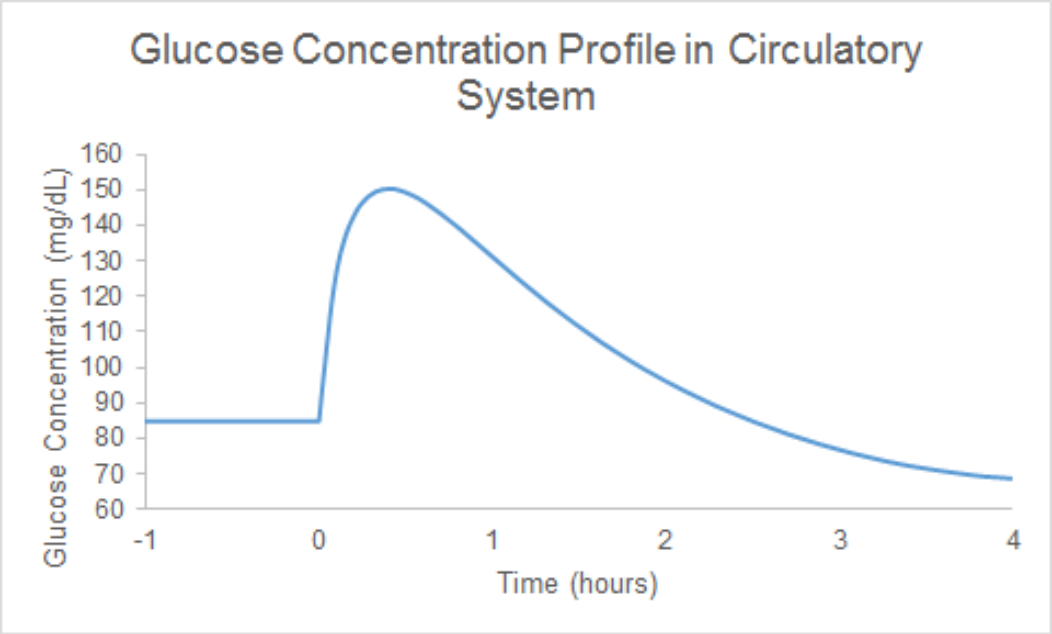

Figure 6: Glucose Concentration Profile after Ingesting 50 g glucose meal.

Insulin and glucagon are assumed to be eliminated by binding to their respective receptors via 1st order elimination. Therefore we assumed that the insulin receptor only existed in the VAT, liver, and skeletal muscle compartments and that insulin is eliminated in those organs. Insulin activates additional glucose absorption terms in the VAT, liver, and skeletal muscle dependent on the changes of insulin concentrations within respective compartments baseline insulin concentrations. Glucagon is eliminated in the liver compartment and increases the glucose secretion term from the liver via glycogenolysis. We assume that there is an infinite storage of glycogen within the liver through successive meals.

We modeled the variable secretion and inhibition of insulin and glucagon as well as their effects on specific organs with effect modeling and fractional bound terms from the respective hormone concentration baselines. The dissociation constant was adjusted within the fractional bound term to adjust the pharmacokinetic profiles of insulin and glucagon within the bloodstream.

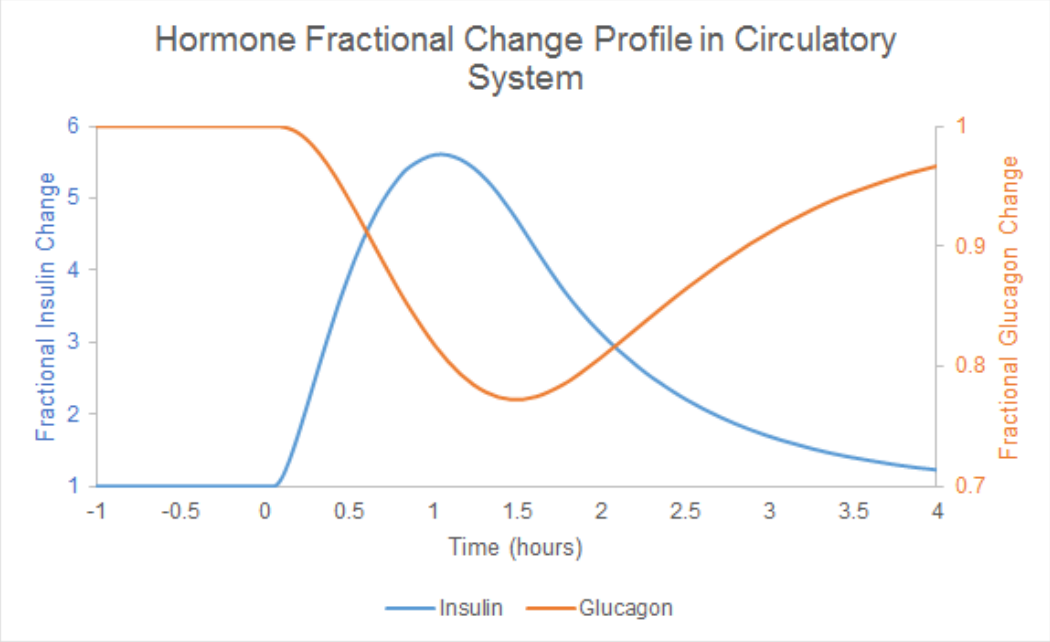

Figure 7: Insulin and Glucagon Fractional Change Profile after 50 g glucose meal.

We then ran the model for over extended periods of 3 regular meals over 24 hours. We added dosages of the same 50 g glucose meal at 0 hour, 4 hour, and 8 hour to represent meals at 8 AM, 12 PM, and 8 PM. The purpose of this was to simulate glucose concentration profiles after a patient consumes only high glucose meals throughout the course of a day. We later ran this model to simulate high-glucose meal consumption over the course of 30 years in order to observe how a high-glucose diet can affect the accumulation of beta amyloid species over an extended period of time.

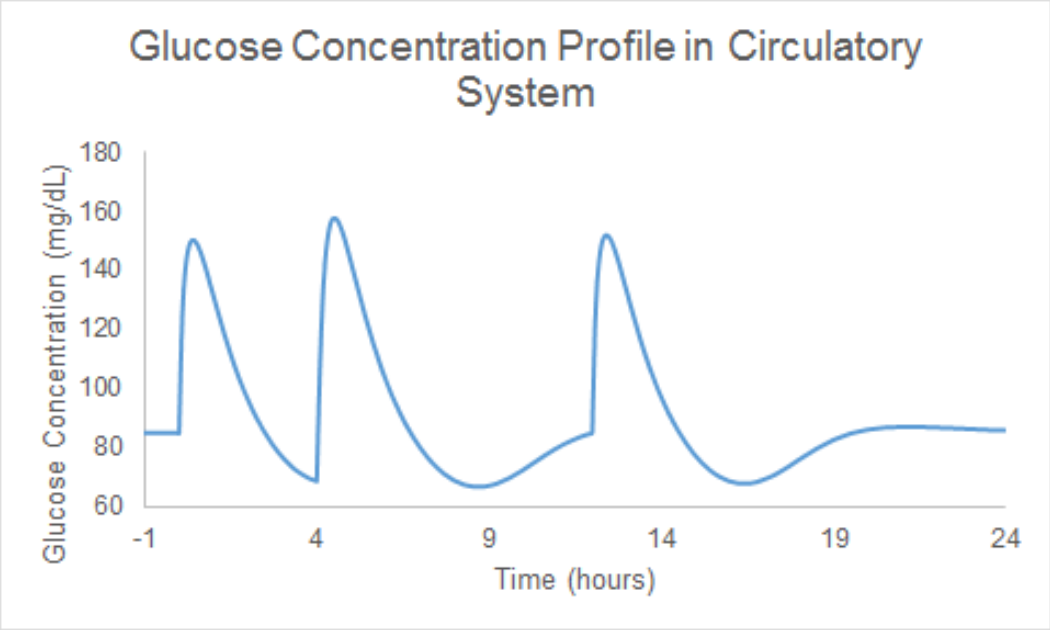

Figure 8: Glucose Concentration Profile after three 50 g glucose meals over the course of a day. Doses were given at 0, 4, and 12 hours. At 0 hours we administer the first meal.

We also modeled a low GI meal, represented as a 5 g glucose meal, so that the glucose concentration would not activate insulin secretion in the model. The glucagon secretion rate would remain constant due to the lack of increased insulin inhibition. These profiles are listed in the figures below.

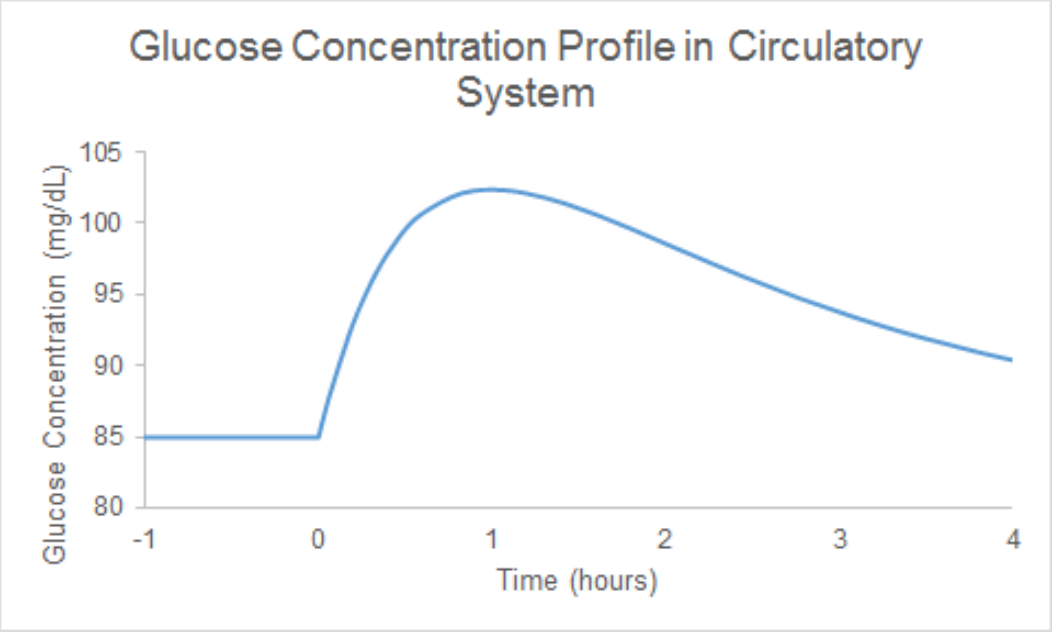

Figure 9: Glucose Concentration Profile in Circulatory System after a 5 g glucose meal. The glucose meal is administered at 0 hour.

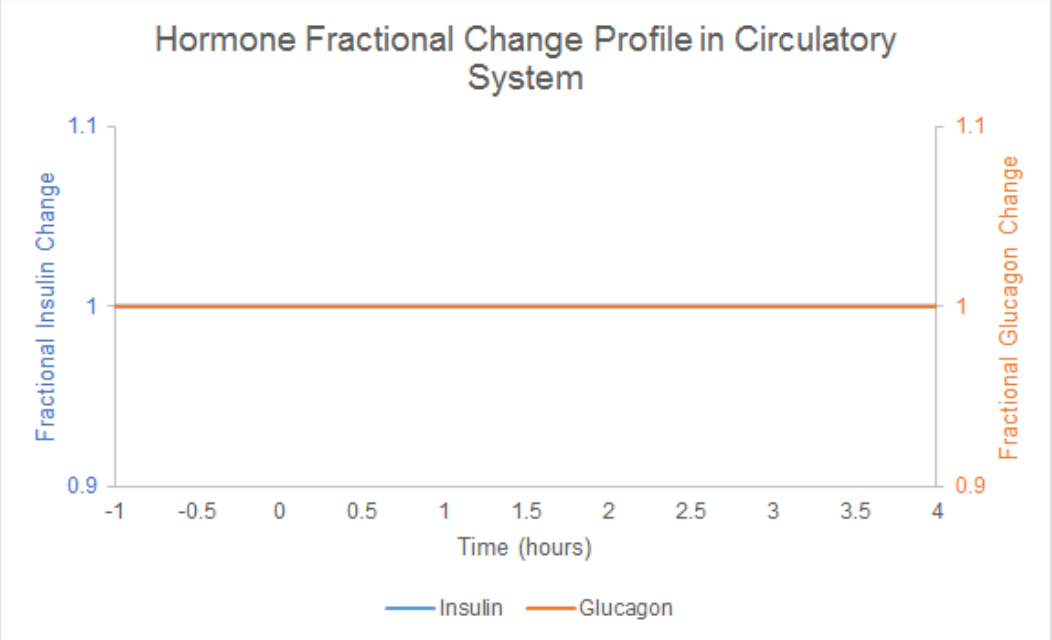

Figure 10: Insulin and Glucagon Fractional Concentration Profiles in Circulatory System after a 5 g glucose meal. Since the pancreas blood glucose concentration did not rise above 110 mg/dL, there is no increase in insulin increase in the system as well as decreased glucagon secretion in the pancreas.

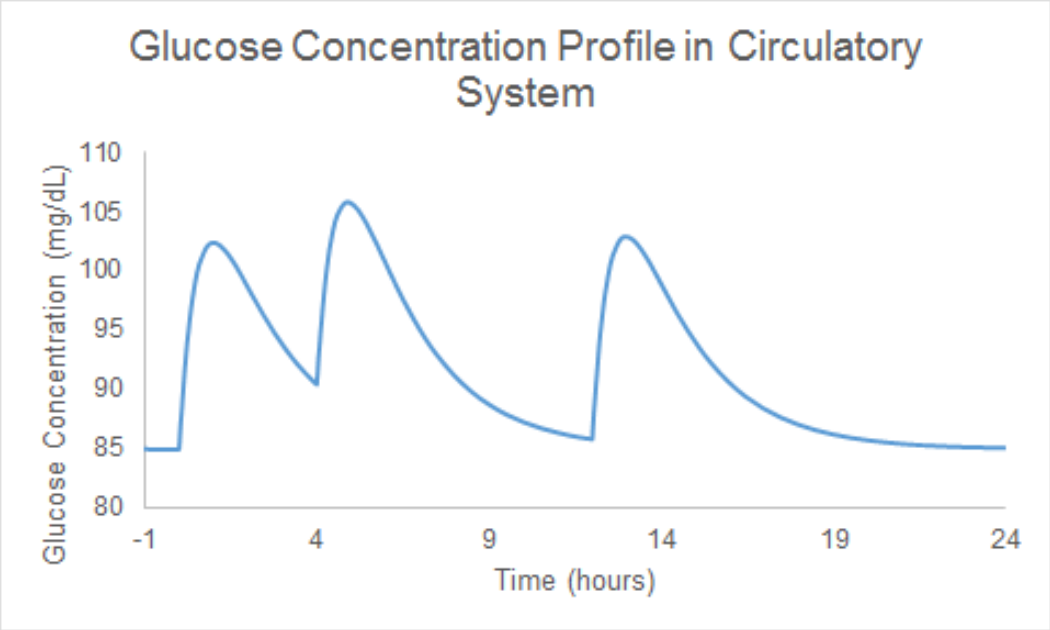

Figure 11: Glucose Concentration Profile in Circulatory System after three 5 g Glucose Meals. Doses were given at 0, 4, and 12 hours. We administered the first meal at 0 hours.

We ran the glucose profiles from the glucose homeostasis model linearly with the beta amyloid and glycation model to determine the effects of glucose concentrations on the glycation of beta amyloids in their respective compartments. To maintain the relative simplicity of our model, we did not simulate the gradual increase in the baseline glucose concentration observed in patients who begin to develop T2DM [1].

BETA AMYLOID & GLYCATION REACTION

We included both glycated and non-glycated beta amyloids in our model in order to observe the effects of a high/low GI meal on their accumulation within specific compartments. We wanted to investigate if we could observe significant accumulation of beta amyloids species in the liver, VAT, and skeletal muscle, and whether the potential of insulin resistance occurred simultaneously or successively in those compartments.

Non-glycated beta amyloids and glycated beta amyloids share the same basic compartment model for glucose homeostasis. We assumed that the primary generation of beta amyloids were from the post-translational modifications of APPs. Therefore, we accounted for beta-amyloid generation as a constant in the model. The tissues with the highest APP expression were the intestines, pancreas, and the brain [47]. We included the APP expression in the brain into our model by adding a generation term into the circulatory system. We assumed that NEP were the most significant source of beta amyloid elimination from the model. Tissues with the highest NEP expression were the intestines, liver, and circulatory system from the brain [48]. Assuming that there is constant NEP expression within tissues, we used the same effect model with fractional bound terms to model beta amyloid elimination. We adjusted the elimination rate constant to match the half-life of beta amyloids in plasma. Although we originally set the generation of beta amyloids to maintain a baseline concentration, research has shown that beta amyloids naturally accumulate in the blood potentially due to decreased expression of tissue-bound NEP in the brain. Therefore we adjusted the elimination of beta amyloids to decrease linearly with time to represent that decrease [49].

Lastly, we modeled the glycation reaction as a 2nd order reaction dependent on the glucose and beta amyloid concentration within the compartment. We assumed the fractional change of the accumulation of beta amyloids to be based on measurements from blood beta amyloid concentrations throughout the lifespan We adjusted the baseline fractional accumulation of beta amyloids to be similar to that of the measured beta amyloid changes over the course of 30 years [50]. Since we assumed no reversible reaction occurs in the model, the glycation rate represented the time for a beta amyloid to form a permanent Amadori product [37].

Results

We applied a sensitivity analysis to the reaction rate constant to determine how glycated beta amyloid concentrations are affected by a high and low GI meal. We also applied the same analysis to the perfusion rate of glucose from the intestines to the VAT to observe how the increased perfusion of VAT would affect the accumulation of glycated amyloid beta concentrations.

We completed the sensitivity analyses on the effect of the glycation reaction rate (krxn) and perfusion flow rate (Q) by multiplying the rate values by factors of 0.01, 0.02, 0.05, 0.1, 0.2, 0.5, 1, 2, 5, and 10. We simulated consumption of high-glucose meals over the course of 30 years to observe the fractional changes of non-glycated beta amyloids and glycated beta amyloids within the model. To decrease computing time, we stored only the beta amyloid and glycated beta amyloid fractional changes at the end of each day.

VARIABLE REACTION RATE

We repeated the high GI meals over the course of 30 years to observe any significant fractional changes between the variable glycation rates. The results can be seen below in *Figure 12-15*.

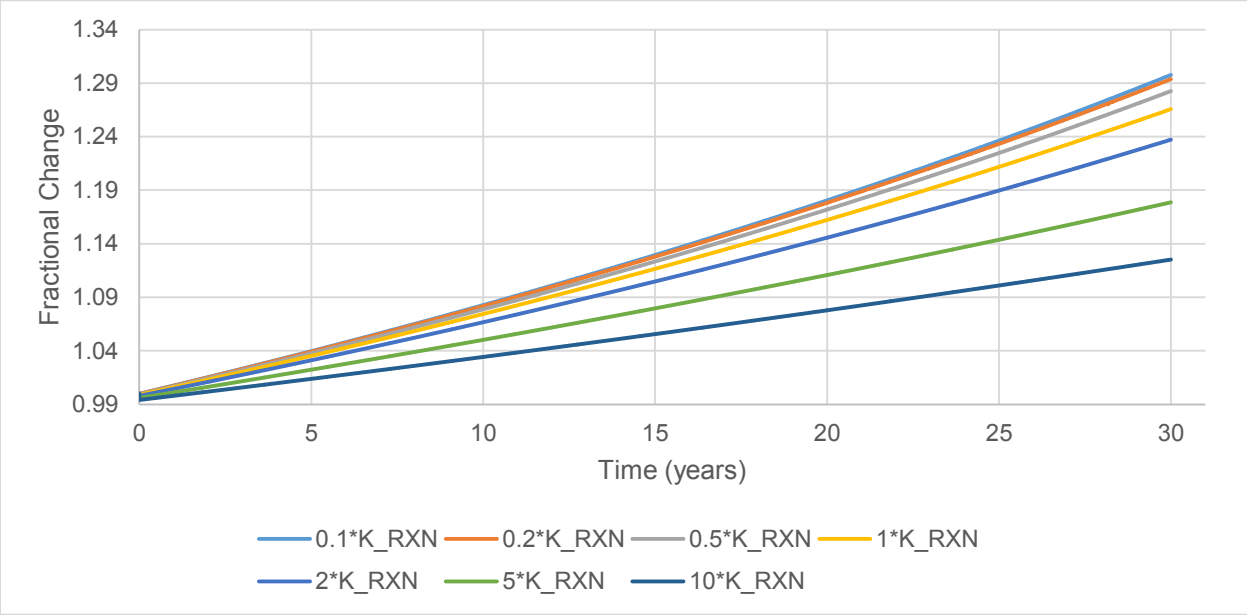

Figure 12: Fractional Change of Beta Amyloid Concentrations in Blood Circulatory System with 50 g Glucose Meal. The fractional change represents the change increase from the baseline beta amyloid concentration at time 0.

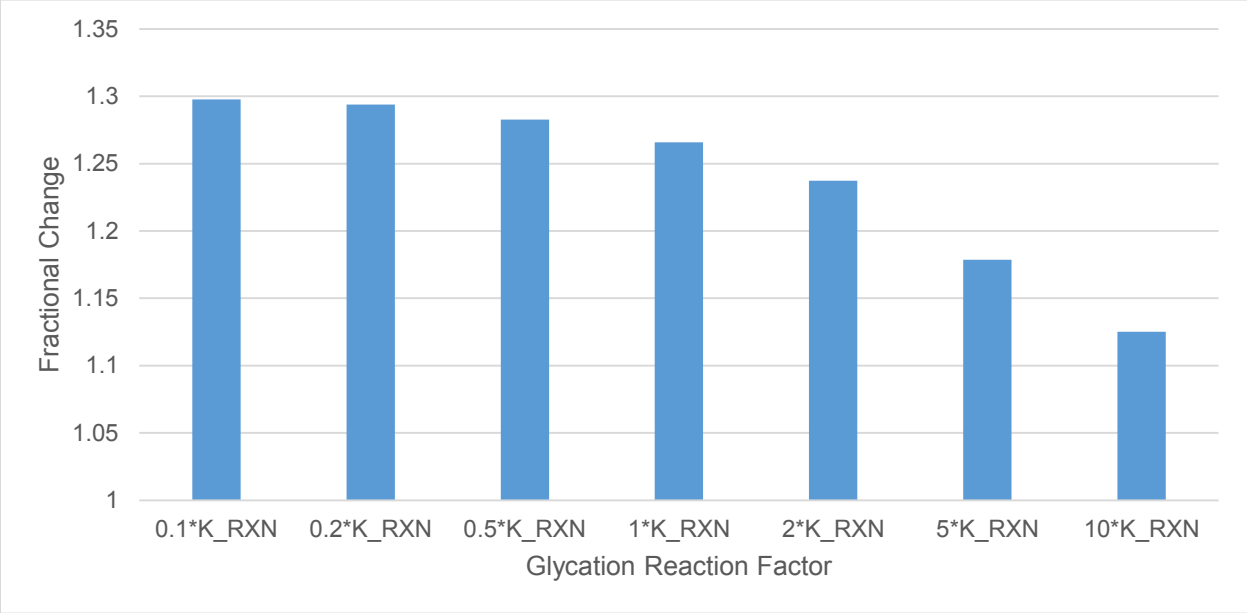

Figure 13: Effect of Glycation Rate on Final Fractional Change of Beta Amyloid with 50 g Glucose Meal. We varied the glycation rate using a sensitivity analysis at the end of 30 years.

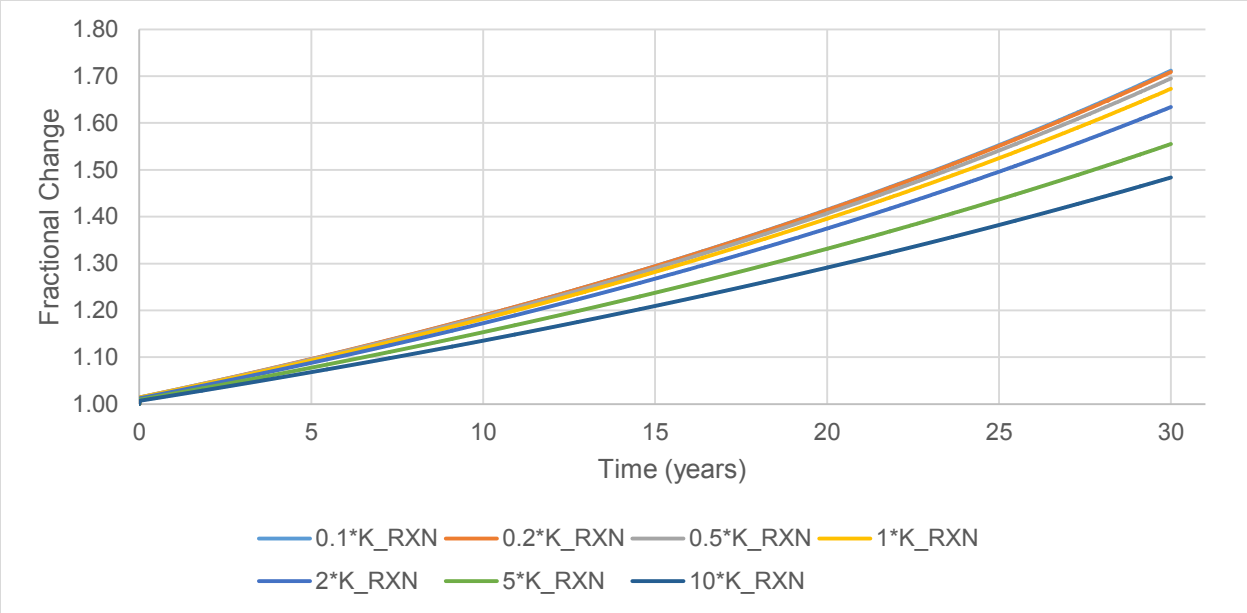

Figure 14: Fractional Change of Glycated Beta Amyloids in Blood Circulatory System with 50 g Glucose Meal. The fractional change represents the fractional increase of beta amyloid concentrations compared to baseline beta amyloid concentrations at time 0.

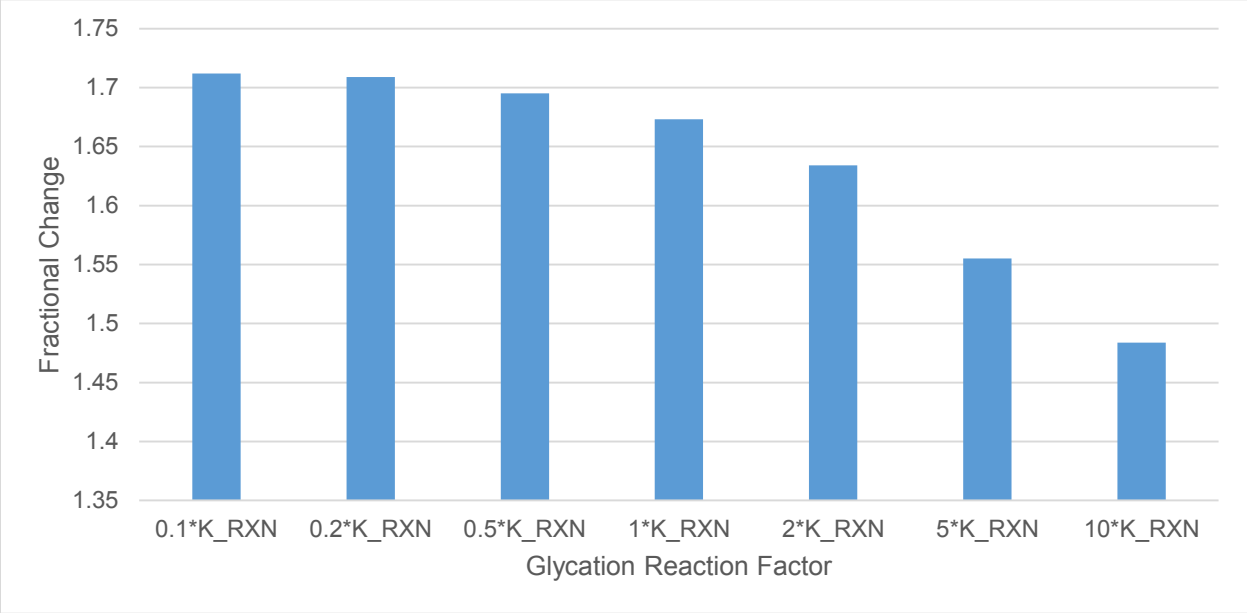

Figure 15: Effect of Glycation Rate on Final Fractional Change of Glycated Beta Amyloid with 50 g Glucose Meal. We varied the glycation rate using a sensitivity analysis at the end of 30 years. The fractional change represents the fractional increase from baseline concentrations.

The reaction rate that achieved the highest fractional change of glycated beta amyloids and non-glycated beta amyloids was 0.1*krxn resulting in a 1.71 and 1.30 fractional increase respectively. The final glycated beta amyloid fractional change decreased as the krxn multiplier

increased. The same behavior was observed for the non-glycated beta amyloid final fractional changes.

We also compared the accumulation of glycated beta amyloids within the VAT, liver, and skeletal muscle across the variable glycation rate seen in *Figure 16*.

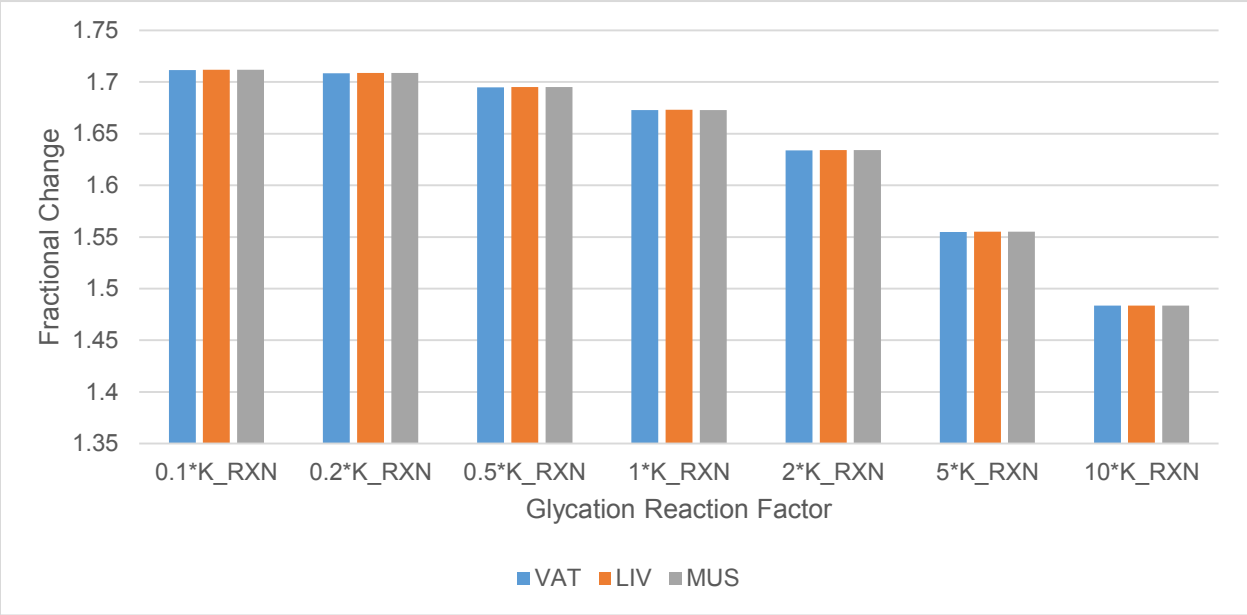

Figure 16: Glycation Rate Effect on Final Fractional Change of Glycated Beta Amyloid with 50 g Glucose Meal in Compartments. We varied the glycation rate using a sensitivity analysis after 30 years. The fractional change represents the fractional increase from baseline concentrations.

We observed that the VAT, liver, and skeletal muscle compartments appear to experience the same final concentration trends in relation to the circulatory system final glycated beta amyloid concentrations). Between the compartments, the liver had the highest glycated beta amyloid fractional changes, then the skeletal muscle, then the VAT. The differences between the organ compartments also appeared to diminish as the glycation rate increased.

We repeated the glycation rate sensitivity analysis with a 5 g glucose meal over the course of 30 years. The results can be seen below in *Figure 17-18*.

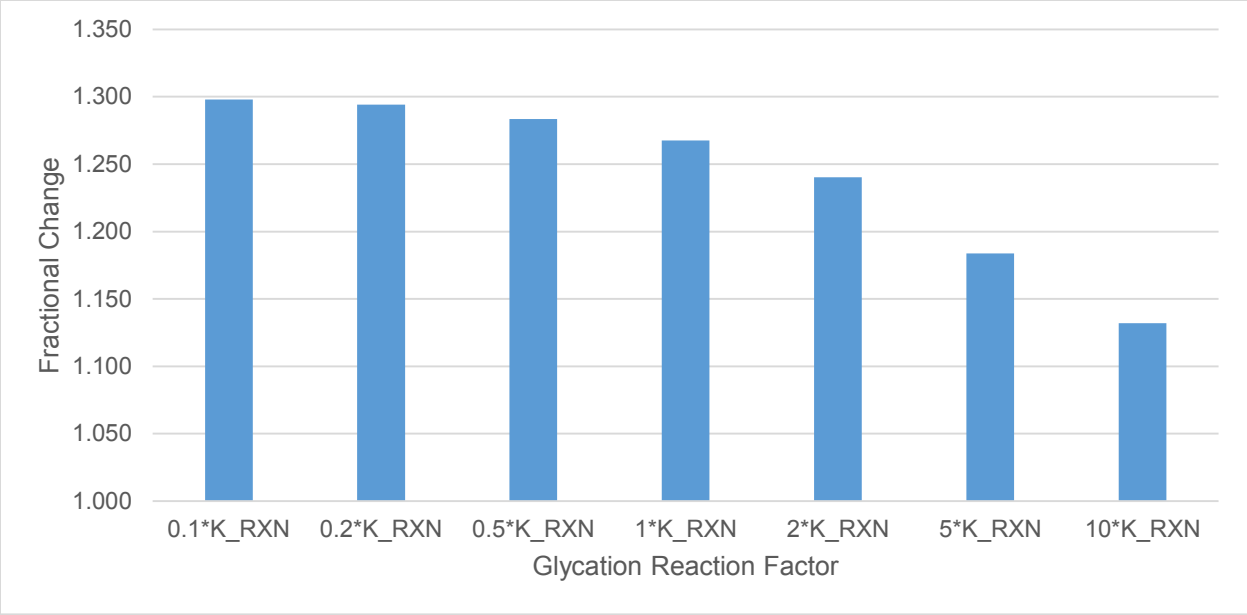

Figure 17: Glycation Rate Effect on Final Fractional Change of Beta Amyloid with 5 g Glucose Meal. We varied the glycation rate using a sensitivity analysis. The fractional change represents the fractional increase from baseline concentrations.

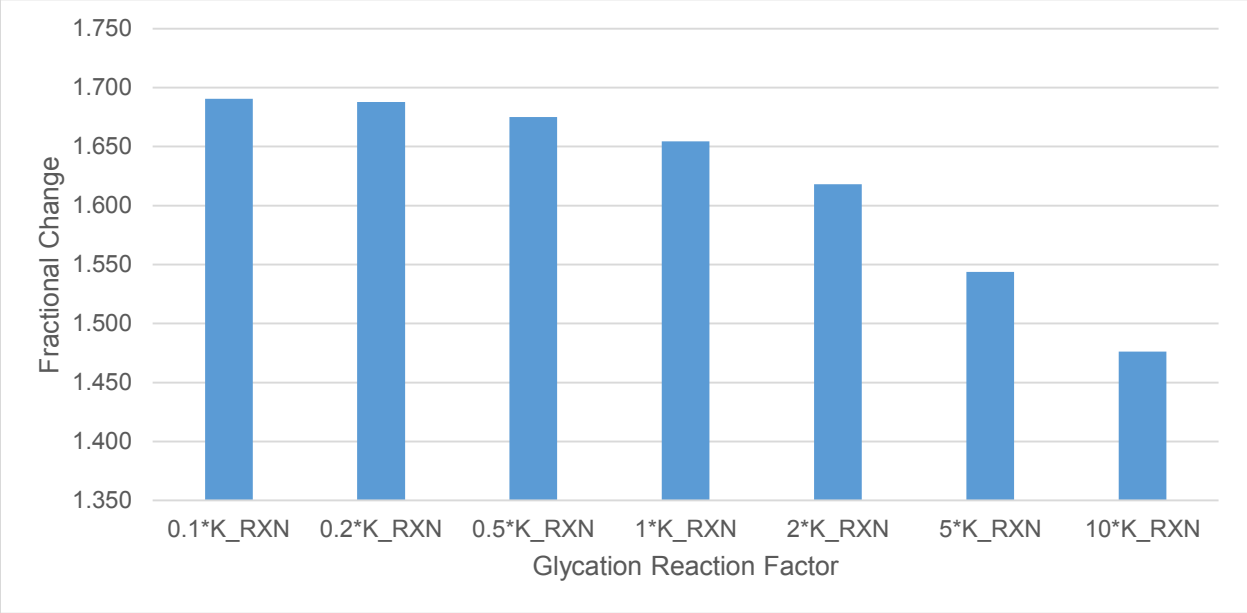

Figure 18: Glycation Rate Effect on Final Fractional Change of Glycated Beta Amyloid with 5 g Glucose Meal. We varied the glycation rate using a sensitivity analysis. The fractional change represents the fractional increase from baseline concentrations.

As shown in *Figures 17-18*, we observed the same optimal glycation rate behavior for the low GI meal data as we did with the high GI meal data. However, for low GI meals we observed the highest glycated beta amyloid fractional change and non-glycated beta amyloid fraction change to be 1.69 and 1.30 respectively. Despite differences in the meals, the high and low GI

meals resulted in the same highest non-glycated beta amyloid fractional change of 1.30 in the circulatory system compartment. We also observed the differences of glycated beta amyloid fractional changes in low GI meals. The results can be seen in *Figure 19*.

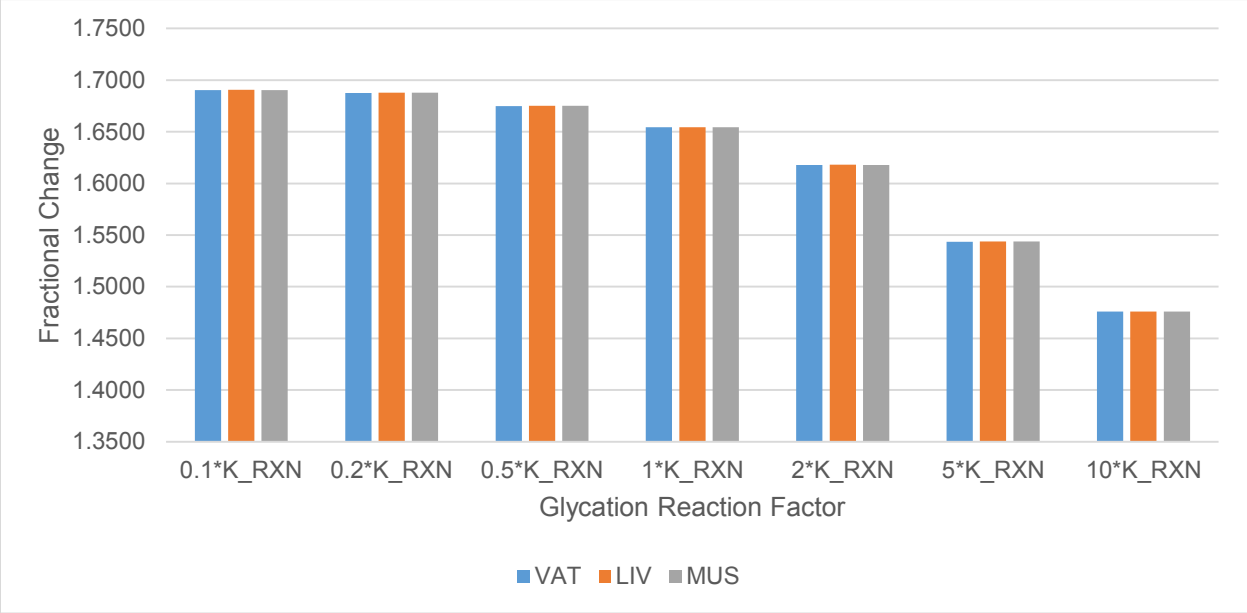

Figure 19: Glycation Rate Effect on Fractional Change of Glycated Beta Amyloid with 5 g Glucose Meal in Compartments. We varied the glycation rate using a sensitivity analysis. The fractional change represents the fractional increase from baseline concentrations.

From *Figure 19* we observed the same behaviors of the final fractional changes of the glycated and non-glycated beta amyloids. Looking at the incremental differences between the compartments, the liver had the highest fractional change, then the skeletal muscle, then the VAT. These results suggest that the accumulation of beta amyloid species in the blood compartments of the organs may rise uniformly, and that insulin resistance may occur simultaneously within organs.

VARIABLE PERFUSION RATE

We analyzed the effect of perfusion from the VAT compartment to the intestines compartment after a single meal of 50 g glucose meal. The results can be seen in *Figure 20*.

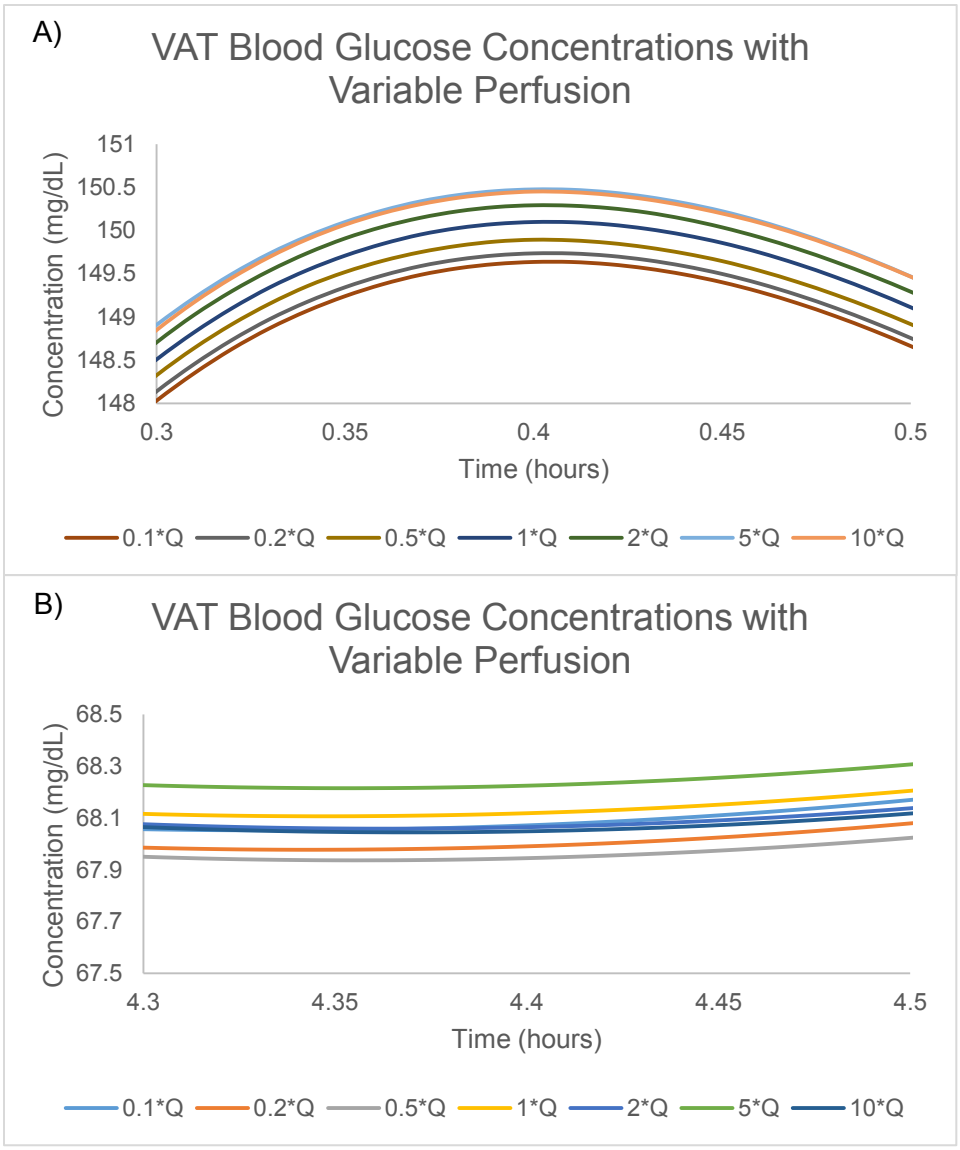

Figure 20: Max and Min Glucose Concentrations in VAT Compartment. (A) exhibits the different maximum concentrations in VAT after a high glucose meal by varying perfusion rate. (B) exhibits the different minimum concentrations in VAT after a high glucose meal with same variation.

The perfusion of glucose flow into the VAT from the intestines compartment resulted in minimal variance between maximum and minimum glucose concentrations in the VAT compartment after a high glucose meal. The VAT compartment reached its maximum glucose concentration at the baseline perfusion flow rate. Increasing and decreasing the perfusion rate both decreased the maximum VAT glucose concentration. We also observed similar behavior in the minimum VAT glucose concentrations.

We varied the perfusion flow rate from the intestine compartment to the VAT compartment in a sensitivity analysis described earlier. While repeating high GI meals over the course of 30 years, we observed an optimal maximal accumulation of glycated and non-glycated beta amyloids in the circulatory system compartment. The results can be seen in *Figure 21-22*.

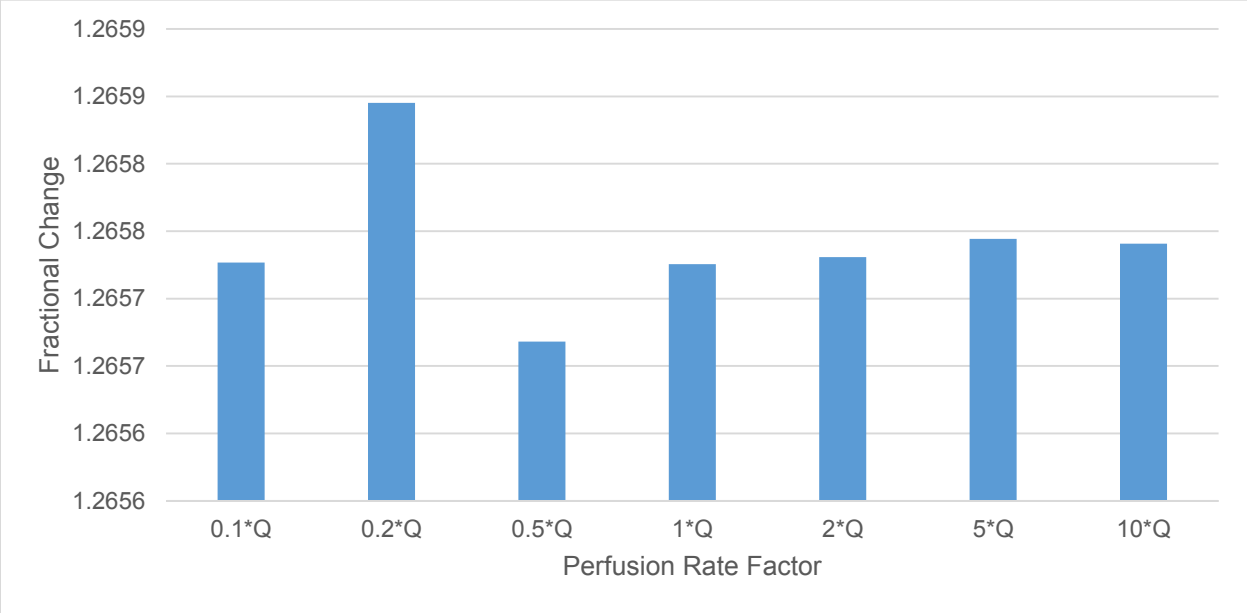

Figure 21: Perfusion Rate Effect on Final Fractional Change of Beta Amyloid with 50 g Glucose Meal. We varied the perfusion rate using a sensitivity analysis from the glucose in the intestines to the VAT. The fractional change represents the fractional increase from baseline concentrations.

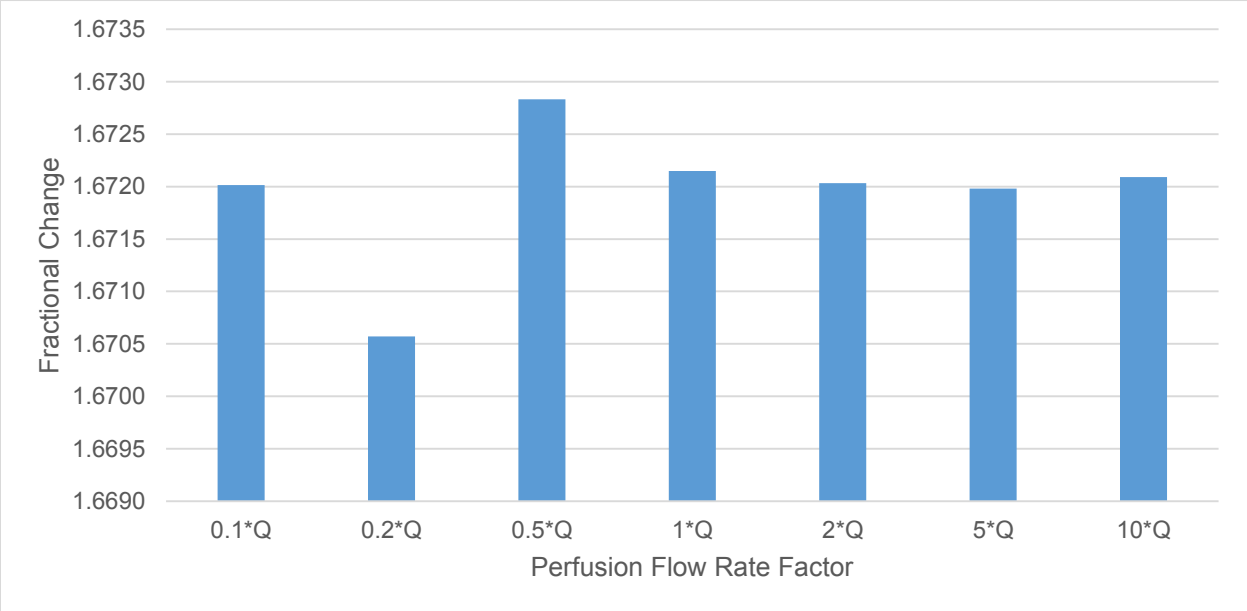

Figure 22: Perfusion Rate Effect on Final Fractional Change of Glycated Beta Amyloid with 50 g Glucose

Meal. We varied the perfusion rate using a sensitivity analysis from the glucose in the intestines to the VAT. The fractional change represents the fractional increase from baseline concentrations.

Keeping the glycation rate constant to 1*krxn, we observed that the highest fractional change of glycated beta amyloids at 0.5*Q and 1.673. However, we observed an inverse relationship between the maximal and minimal final fractional change values of the glycated and non-glycated beta amyloids. The minimal fractional change of non-glycated beta amyloids corresponded to the maximal fractional change of glycated beta amyloids across the sensitivity analysis. Additionally, the differences between the final fractional changes varied significantly less than the variable glycation rate values, with changes varying in the tenths rather than the ten-thousandths.

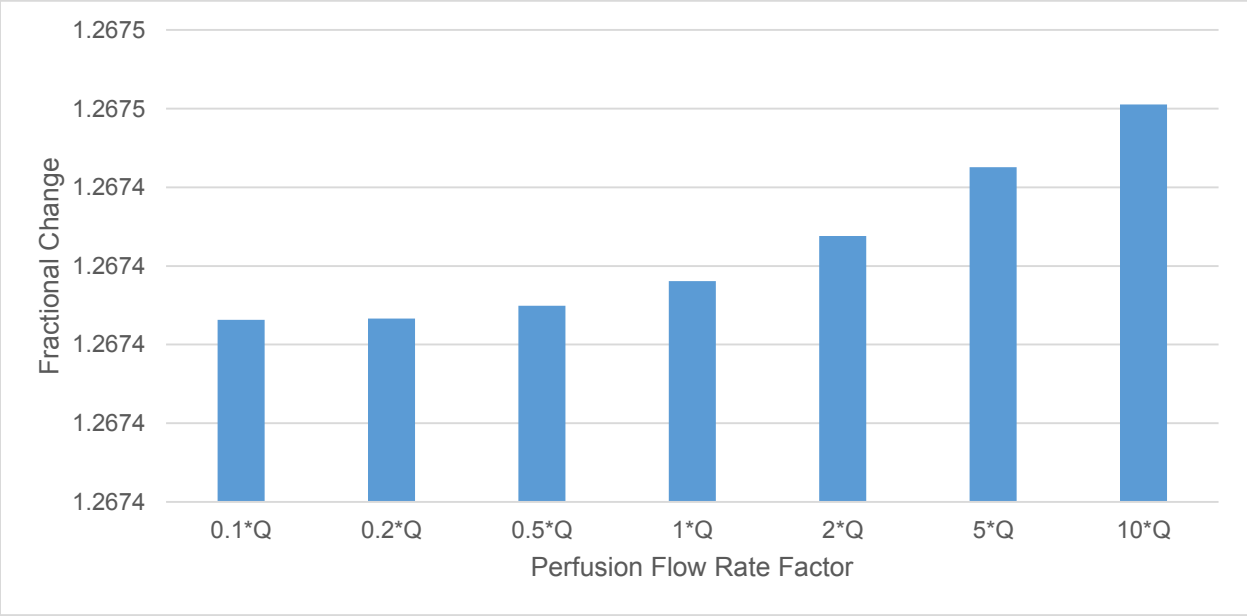

Figure 23: Perfusion Rate Effect on Final Fractional Change of Beta Amyloid with 5 g Glucose Meal. We varied the perfusion rate using a sensitivity analysis from the glucose in the intestines to the VAT. The fractional change represents the fractional increase from baseline concentrations.

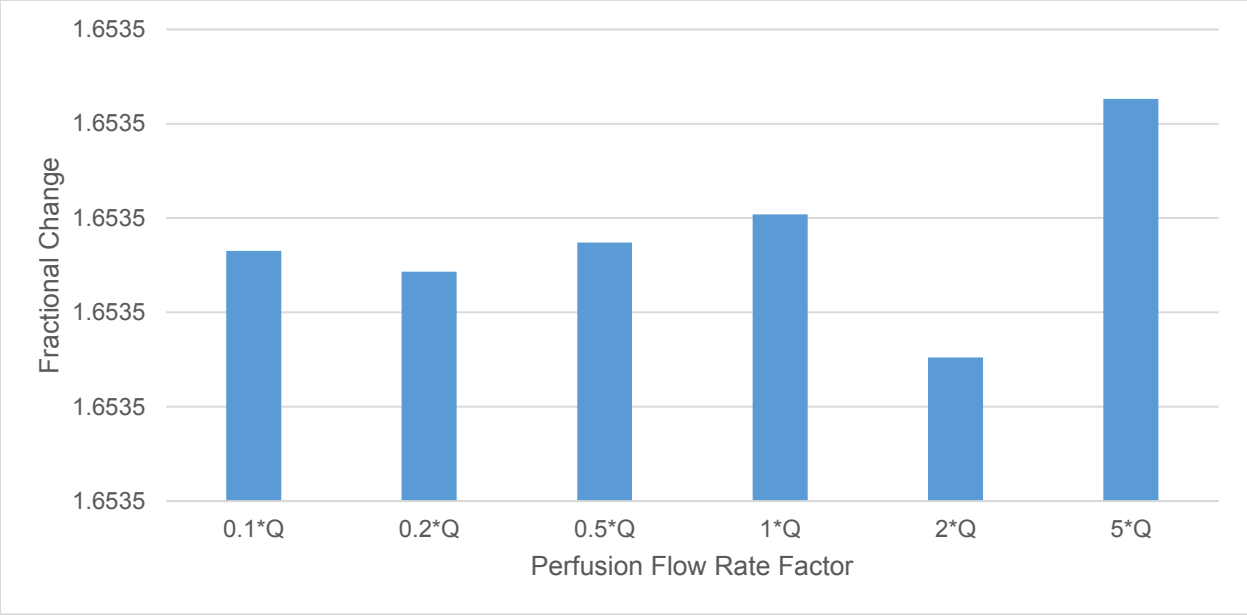

Figure 24: Perfusion Rate Effect on Final Fractional Change of Glycated Beta Amyloid with 5 g Glucose Meal in Organs. We varied the perfusion rate using a sensitivity analysis from the glucose in the intestines to the VAT. The fractional change represents the fractional increase from baseline concentrations.

We ran the variable perfusion analysis with a low GI meal as seen in *Figure 23-24*. We observed that the glycated beta amyloid final fractional changes varied insignificantly between the sensitivity factors. The perfusion rate appeared to have little effect on the final non-glycated beta amyloid fractional as well, but the final fractional change did increase in response to increasing perfusion rate.

In Figure 25, we also observed insignificant glycated beta amyloid fractional change differences between the VAT, liver, and skeletal muscle compartments.

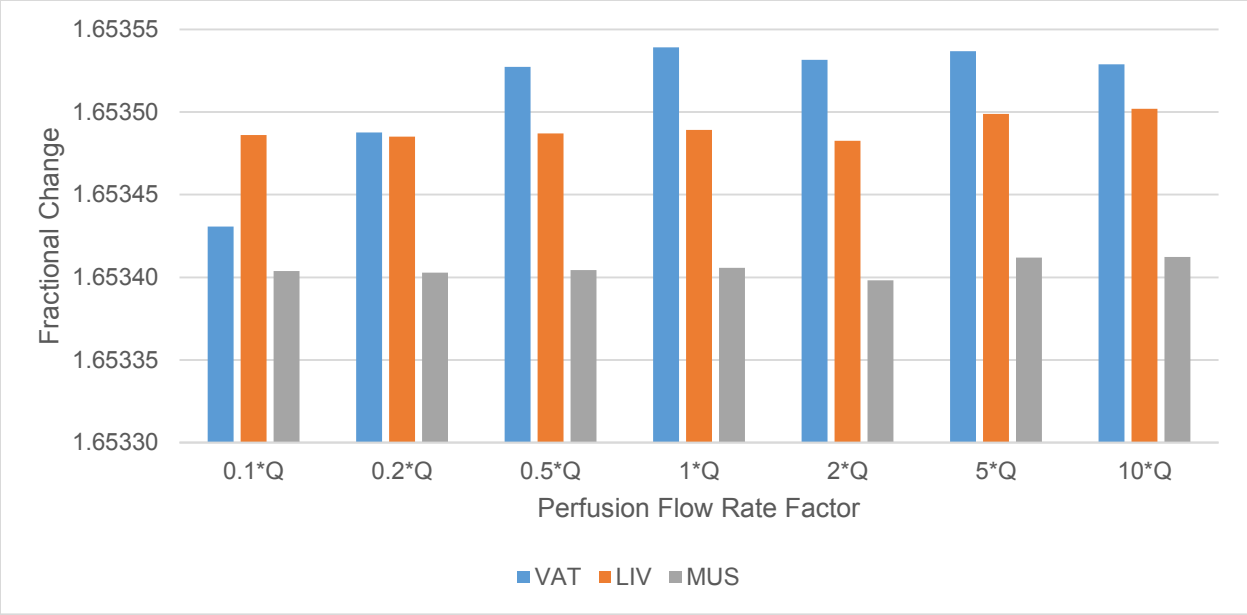

Figure 25: Perfusion Rate Effect on Final Fractional Change of Glycated Beta Amyloid with 5 g Glucose Meal in Compartments. We varied the perfusion rate using a sensitivity analysis from the glucose in the intestines to the VAT. The fractional change represents the fractional increase from baseline concentrations.

With a low GI meal, the VAT glycated beta amyloid concentrations appeared to increase as the perfusion rate increased from 0.1*Q. The other glycated beta amyloid concentrations did not appear to change as much as that in the VAT compartment. We observed some changes in those compartments across the perfusion flow rates, but considering the scale smaller than ten-thousandths we deemed it insignificant.

Discussion

The purpose of this model was to determine how the effects of high and low GI meals affected the final fractional change of beta amyloid species in blood compartments. Between the high and low GI meals, we applied a sensitivity analysis to the glucose perfusion from the intestines to the VAT blood compartments and to the glycation rate. We specifically wanted to observe the accumulation of beta amyloid species in the VAT, liver, and skeletal muscles due to their important role towards the pathogenesis of insulin resistance in T2DM.

EFFECT OF HIGH AND LOW GI MEALS

From the results in *Figure 12*, we observed that there was an optimal glycation rate that yielded the greatest concentration of glycated beta amyloids in the model. The degree to which the glycation rate affected the accumulation of glycated beta amyloids depended on the amount of glucose in the meal. We observed greater variability as the glycation rate increased, but as the glycation rate decreased below 0.1*krxn, the final fractional change of the glycated beta amyloids did not appear to vary as greatly. Furthermore, we observed even less variability in the final fractional changes of beta amyloid species with a low GI meal. The circulatory system's non-glycated and glycated beta amyloid fractional changes appeared to mirror fractional changes to those of the VAT, liver, and skeletal muscle compartments. We concluded that the glycation rate had an overall effect on the entire system’s rate of accumulation rather than specifically within certain compartments.

The type of GI meal did affect the maximal glycated beta amyloid fractional changes. We observed a 0.02 difference between the maximal glycated beta amyloid fractional changes at a

high glucose meal and a low one. Although high glucose meals are associated with higher AGEs in the body, it is unclear how much of a difference a 0.02 fractional change makes.

The changes to the perfusion rate between the intestines and VAT compartments had less of an impact on the final glycated beta amyloid fractional change than that of the changes to the glycation rate. The final fractional changes boiled down to a difference of a magnitude of millionths versus thousandths respectively. Although we did observe greater perfusion of glucose within the VAT compartment with an increase of perfusion rate, it appeared to have little effect on the final glycated fractional changes between the compartments. Therefore perfusion between the blood compartments does not appear to contribute significantly to the accumulation of beta amyloid species within organs, and thus contribute significantly towards the pathogenesis of insulin resistance.

The accumulation of beta amyloids in these compartments may elucidate the cellular development of T2DM over time due to a high glycemic index diet. As mentioned before, beta amyloids can not only exert insulin insensitivity but also inflammation and steatosis into organ tissue, some of many physiological symptoms in T2DM patients. We propose the potential cellular effects beta amyloids may exert on cells in *Figure 26*.

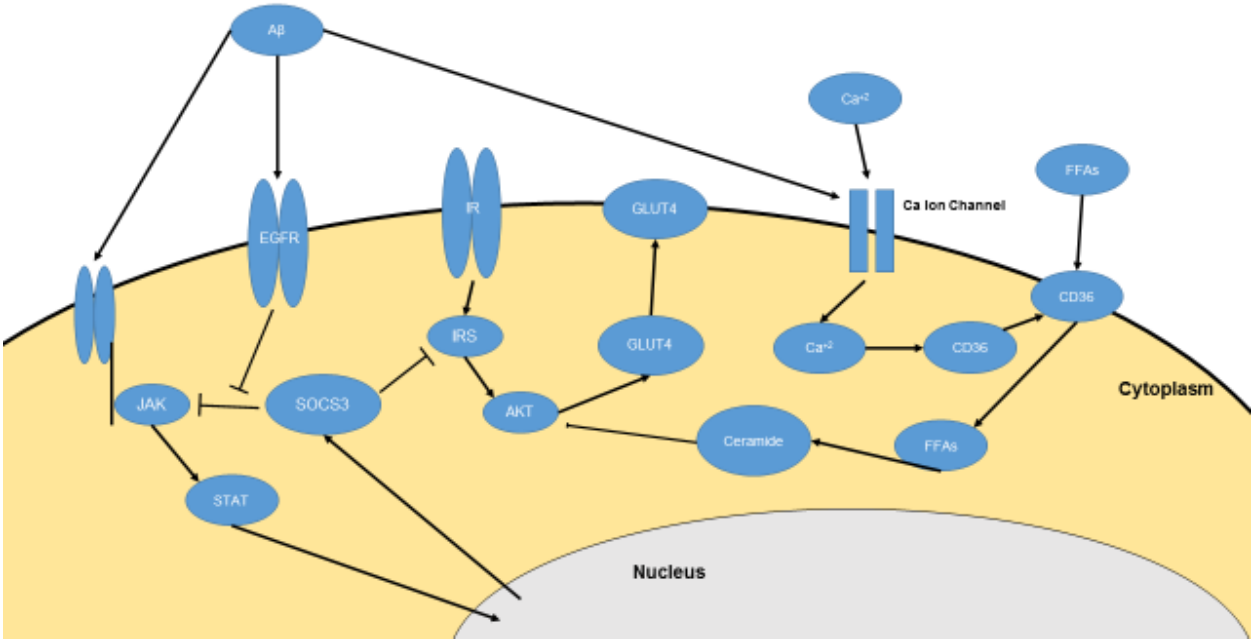

Figure 26: Effects of beta amyloid onto cellular mechanisms. Beta amyloids can directly bind to receptors or bind to cell surface membranes to elicit effects on cellular processes that affect inflammation and FFA absorption.

Figure 26 shows that beta amyloids can exert multiple effects such as inflammation and potentially FFA accumulation by binding to specific receptors on cell membranes. Beta amyloids can activate the JAK/STAT pathway to induce insulin resistance via inflammation through both SOCS inactivation and accumulation. They can also induce cellular FFA absorption which can induce the accumulation of harmful metabolites such as ceramides that affect Akt processes, which include insulin signaling. There is currently no research on whether inflammation or FFA accumulation contributes more to insulin resistance in the tissue, nor whether one symptom begets the other. Nonetheless, it is important to note that beta amyloids can induce both of these effects.

Based on the results, we observed little variance in the final fractional changes of beta amyloid species between the VAT, liver, and skeletal muscle blood compartments. Although glycation rate caused the most variance of final beta amyloid fractional changes, the model did not account for the absorption of beta amyloid species into tissue compartments.

CODE IMPROVEMENTS

To improve the physiological accuracy of the model, future models should include extra compartments that represent the organs' interstitial fluid volumes. Regarding the uptake of glycated beta amyloids into tissue, researchers have discovered that AGEs upregulate RAGEs to absorb more AGEs into tissue [50]. Depending on how sensitive RAGEs are towards AGE concentrations in the bloodstream, small changes to the glycated beta amyloid concentrations may promote increased overall tissue beta amyloid concentrations. From the blood compartments beta amyloids should absorb into the tissue volume compartments in a protein-binding dependent manner. Although beta amyloid concentrations in the blood can correlate with the potential accumulated beta amyloids in the organ tissue, it is unclear whether the glycation rate is the most significant factor towards the critical accumulation of beta amyloids within the tissues.

Further improvements made to the code should include a distinction between the beta amyloids generated from APP and beta amyloid-protein interactions. An increase of beta amyloids may cause the generation of more beta amyloids within compartments that do not generate APP in the tissue. Also, the generation of beta amyloids should occur in APP expressing tissue (circulatory system, intestine, and pancreas) compartments. The glucose perfusion from the intestine to the VAT would more accurately be modeled as flow from the intestines blood compartment to the VAT tissue compartment.

References

1. "Diabetes." *World Health Organization*, World Health Organization, https://www.who.int/news-room/fact-sheets/detail/diabetes.
2. Meyts, Pierre De. "The Insulin Receptor and Its Signal Transduction Network." *Endotext [Internet]*., U.S. National Library of Medicine, 27 Apr. 2016, https://www.ncbi.nlm.nih.gov/books/NBK378978/.
3. "Does Insulin Make You Fat?" Sigma Nutrition, 10 Dec. 2016, https://sigmanutrition.com/does-insulin-make-you-fat/.
4. A Cherrington, A.d., et al. "Insulin Action on the Liver in Vivo." *Biochemical Society Transactions*, vol. 35, no. 5, 2007, pp. 1171–1174., doi:10.1042/bst0351171.
5. Rix, Iben. "Glucagon Physiology." *Endotext [Internet]*., U.S. National Library of Medicine, 16 July 2019, https://www.ncbi.nlm.nih.gov/books/NBK279127/.
6. Quesada, Ivan, et al. "Physiology of the Pancreatic α-Cell and Glucagon Secretion: Role in Glucose Homeostasis and Diabetes in: Journal of Endocrinology Volume 199 Issue 1 (2008)." *Journal of Endocrinology*, BioScientifica, 5 Aug. 2018, https://joe.bioscientifica.com/view/journals/joe/199/1/5.xml.
7. Abdul-Ghani, Muhammad A., and Ralph A. Defronzo. "Pathogenesis of Insulin Resistance in Skeletal Muscle." *Journal of Biomedicine and Biotechnology*, vol. 2010, 2010, pp. 1–19., doi:10.1155/2010/476279.
8. "Diabetes." *World Health Organization*, World Health Organization, https://www.who.int/news-room/fact-sheets/detail/diabetes.
9. Frayn, Keith N. "Adipose Tissue and the Insulin Resistance Syndrome." *Proceedings of the Nutrition Society*, vol. 60, no. 3, 5 Mar. 2001, pp. 375–380., doi:10.1079/pns200195.
10. Muhammad A. Abdul-Ghani and Ralph A. DeFronzo, "Pathogenesis of Insulin Resistance in Skeletal Muscle," Journal of Biomedicine and Biotechnology, vol. 2010, Article ID 476279, 19 pages, 2010. https://doi.org/10.1155/2010/476279.
11. McFarlan, Jay T et al. "In vivo, fatty acid translocase (CD36) critically regulates skeletal muscle fuel selection, exercise performance, and training-induced adaptation of fatty acid oxidation." *The Journal of biological chemistry* vol. 287,28 (2012): 23502-16. doi:10.1074/jbc.M111.315358
12. Goudriaan, Jeltje R., et al. "CD36 Deficiency Increases Insulin Sensitivity in Muscle, but Induces Insulin Resistance in the Liver in Mice." *Journal of Lipid Research*, vol. 44, no. 12, 2003, pp. 2270–2277., doi:10.1194/jlr.m300143-jlr200.
13. Cytokines and chemokines: At the crossroads of cell signalling and inflammatory disease Turner M.D., Nedjai B., Hurst T., Pennington D.J.

(2014) *Biochimica et Biophysica Acta - Molecular Cell Research*, 1843 (11) , pp. 2563-2582.

14. Wu, Huaizhu, and Christie M. Ballantyne. "Skeletal Muscle Inflammation and Insulin Resistance in Obesity." *Journal of Clinical Investigation*, vol. 127, no. 1, Mar. 2017, pp. 43–54., doi:10.1172/jci88880.

15. Torisu, Takehiro, et al. "The Dual Function of Hepatic SOCS3 in Insulin Resistance in Vivo." *Genes to Cells*, vol. 12, no. 2, 2 Feb. 2007, pp. 143–154., doi:10.1111/j.1365-2443.2007.01044.x.

16. Zhang, Yi, et al. "Amyloid-β Induces Hepatic Insulin Resistance In Vivo via JAK2." *Diabetes*, American Diabetes Association, 1 Apr. 2013, diabetes.diabetesjournals.org/content/62/4/1159.

17. Corbit KC, Camporez JPG, Edmunds LR, Tran JL, Vera NB, Erion DM, Deo RC, Perry RJ, Shulman GI, Jurczak MJ, Weiss EJ. Adipocyte JAK2 Regulates Hepatic Insulin Sensitivity Independently of Body Composition, Liver Lipid Content, and Hepatic Insulin Signaling. Diabetes. 2018;**67**(2):208–21. Epub 2017/12/06. doi: 10.2337/db17-0524. PubMed PMID: 29203511.

18. Akter, Kawser, et al. "Diabetes Mellitus and Alzheimer's Disease: Shared Pathology and Treatment?" British Journal of Clinical Pharmacology, vol. 71, no. 3, Mar. 2011, pp. 365–376., doi:10.1111/j.1365-2125.2010.03830.x.

19. Blanchard, B., Thomas, V. and Ingram, V. (2002). Mechanism of membrane depolarization caused by the Alzheimer Aβ1–42 peptide. *Biochemical and Biophysical Research Communications*, 293(4), pp.1197-1203.

20. Fawaz Alasmari, Musaad A. Alshammari, Abdullah F. Alasmari, Wael A. Alanazi, and Khalid Alhazzani, "Neuroinflammatory Cytokines Induce Amyloid Beta Neurotoxicity through Modulating Amyloid Precursor Protein Levels/Metabolism," BioMed Research International, vol. 2018, Article ID 3087475, 8 pages, 2018. https://doi.org/10.1155/2018/3087475.

21. Wang, L., et al. "Epidermal Growth Factor Receptor Is a Preferred Target for Treating Amyloid- -Induced Memory Loss." *Proceedings of the National Academy of Sciences*, vol. 109, no. 41, 2012, pp. 16743–16748., doi:10.1073/pnas.1208011109.

22. Lebrun, P., and E. Van Obberghen. "SOCS Proteins Causing Trouble in Insulin Action." *Acta Physiologica*, vol. 192, no. 1, 2007, pp. 29–36., doi:10.1111/j.1748-1716.2007.01782.x.

23. Yang, Guang, et al. "Central Role of Ceramide Biosynthesis in Body Weight Regulation, Energy Metabolism, and the Metabolic Syndrome." *American Journal of Physiology-Endocrinology and Metabolism*, vol. 297, no. 1, 2009, doi:10.1152/ajpendo.91014.2008.

24. Stratford, Suzanne, et al. “Regulation of Insulin Action by Ceramide.” *Journal of Biological Chemistry*, vol. 279, no. 35, 2004, pp. 36608–36615., doi:10.1074/jbc.m406499200.

25. Osaki, M., et al. “PI3K-Akt Pathway: Its Functions and Alterations in Human Cancer.” *Apoptosis*, vol. 9, no. 6, 2004, pp. 667–676., doi:10.1023/b:appt.0000045801.15585.dd.

26. Turner, Mark D., et al. “Cytokines and Chemokines: At the Crossroads of Cell Signalling and Inflammatory Disease.” *Biochimica Et Biophysica Acta (BBA) - Molecular Cell Research*, vol. 1843, no. 11, 2014, pp. 2563–2582., doi:10.1016/j.bbamcr.2014.05.014.

27. Rodrigue, K. M., et al. “ -Amyloid Burden in Healthy Aging: Regional Distribution and Cognitive Consequences.” *Neurology*, vol. 78, no. 6, Jan. 2012, pp. 387–395., doi:10.1212/wnl.0b013e318245d295.

28. Chen, Hong, et al. “Living near Major Roads and the Incidence of Dementia, Parkinson's Disease, and Multiple Sclerosis: a Population-Based Cohort Study.” The Lancet, vol. 389, no. 10070, 4 Jan. 2017, pp. 718–726., doi:10.1016/s0140-6736(16)32399-6.

29. O'Brien, Richard J, and Philip C Wong. “Amyloid precursor protein processing and Alzheimer's disease.” *Annual review of neuroscience* vol. 34 (2011): 185-204. doi:10.1146/annurev-neuro-061010-113613

30. Baldassarre, Maurizio et al. “Amyloid β-peptides 1-40 and 1-42 form oligomers with mixed β-sheets.” *Chemical science* vol. 8,12 (2017): 8247-8254. doi:10.1039/c7sc01743j

31. Akter, Kawser et al. “Diabetes mellitus and Alzheimer's disease: shared pathology and treatment?.” *British journal of clinical pharmacology* vol. 71,3 (2011): 365-76. doi:10.1111/j.1365-2125.2010.03830.x

32. Baranello, Robert J et al. “Amyloid-beta protein clearance and degradation (ABCD) pathways and their role in Alzheimer's disease.” *Current Alzheimer research* vol. 12,1 (2015): 32-46. doi:10.2174/1567205012666141218140953

33. Hersh, Louis, and David Rodgers. “Neprilysin and Amyloid Beta Peptide Degradation.” *Current Alzheimer Research*, vol. 5, no. 2, Jan. 2008, pp. 225–231., doi:10.2174/156720508783954703.

34. Baranello, Robert J et al. “Amyloid-beta protein clearance and degradation (ABCD) pathways and their role in Alzheimer's disease.” *Current Alzheimer research* vol. 12,1 (2015): 32-46. doi:10.2174/1567205012666141218140953

35. Glenn, Josephine V., and Alan W. Stitt. “The Role of Advanced Glycation End Products in Retinal Ageing and Disease.” *Biochimica Et Biophysica Acta (BBA) - General Subjects*, vol. 1790, no. 10, 2009, pp. 1109–1116., doi:10.1016/j.bbagen.2009.04.016.

36. Münch, G., et al. “Alzheimers Disease – Synergistic Effects of Glucose Deficit, Oxidative Stress and Advanced Glycation Endproducts.” *Journal of Neural Transmission*, vol. 105, no. 4, Feb. 1998, p. 439., doi:10.1007/s007020050069.

37. Grimm, Marcus O. W., et al. “Neprilysin and Aβ Clearance: Impact of the APP Intracellular Domain in NEP Regulation and Implications in Alzheimer’s Disease.” *Frontiers in Aging Neuroscience*, vol. 5, 23 Dec. 2013, doi:10.3389/fnagi.2013.00098.

38. Basta, G. “Advanced Glycation End Products and Vascular Inflammation: Implications for Accelerated Atherosclerosis in Diabetes.” *Cardiovascular Research*, vol. 63, no. 4, 2004, pp. 582–592., doi:10.1016/j.cardiores.2004.05.001.

39. Levi, Boaz, and Moshe J. Werman. “Long-Term Fructose Consumption Accelerates Glycation and Several Age-Related Variables in Male Rats.” *The Journal of Nutrition*, vol. 128, no. 9, Jan. 1998, pp. 1442–1449., doi:10.1093/jn/128.9.1442.

40. Schedin-Weiss, Sophia, et al. “The Role of Protein Glycosylation in Alzheimer Disease.” *FEBS Journal*, vol. 281, no. 1, 2013, pp. 46–62., doi:10.1111/febs.12590.

41. Murphy, M Paul, and Harry LeVine 3rd. “Alzheimer's disease and the amyloid-beta peptide.” *Journal of Alzheimer's disease : JAD* vol. 19,1 (2010): 311-23. doi:10.3233/JAD-2010-1221

42. Emendato, Alessandro et al. “Glycation affects fibril formation of Aβ peptides.” *The Journal of biological chemistry* vol. 293,34 (2018): 13100-13111. doi:10.1074/jbc.RA118.002275

43. Odetti, Patrizio, et al. “Plasma Levels of Insulin and Amyloid β42 Are Correlated in Patients with Amnestic Mild Cognitive Impairment.” *Journal of Alzheimers Disease*, vol. 8, no. 3, May 2005, pp. 243–245., doi:10.3233/jad-2005-8303.

44. Mullins, Roger J et al. “Insulin Resistance as a Link between Amyloid-Beta and Tau Pathologies in Alzheimer's Disease.” *Frontiers in aging neuroscience* vol. 9 118. 3 May. 2017, doi:10.3389/fnagi.2017.00118

45. Grodstein, Gerald P., et al. “Glucose Absorption during Continuous Ambulatory Peritoneal Dialysis.” Kidney International, vol. 19, no. 4, 1981, pp. 564–567., doi:10.1038/ki.1981.53.

46. Jacobsen, S. H., et al. “Changes in Gastrointestinal Hormone Responses, Insulin Sensitivity, and Beta-Cell Function Within 2 Weeks After Gastric Bypass in Non-Diabetic Subjects.” *Obesity Surgery*, vol. 22, no. 7, 2012, pp. 1084–1096., doi:10.1007/s11695-012-0621-4.

47. *Tissue Expression of APP - Summary - The Human Protein Atlas*, Human Protein Atlas, https://www.proteinatlas.org/ENSG00000142192-APP/tissue.

48. *MME Protein Expression Summary - The Human Protein Atlas*, https://www.proteinatlas.org/ENSG00000196549-MME.

49. Zecca, Chiara, et al. "Plasma β-Amyloid 1–42 Reference Values in Cognitively Normal Subjects." *Journal of the Neurological Sciences*, vol. 391, 2018, pp. 120–126., doi:10.1016/j.jns.2018.06.006.

50. Semba, Richard D et al. "Does accumulation of advanced glycation end products contribute to the aging phenotype?." *The journals of gerontology. Series A, Biological sciences and medical sciences* vol. 65,9 (2010): 963-75. doi:10.1093/gerona/glq074

51. Peters, Sheila Annie. *Physiologically-Based Pharmacokinetic (PBPK) Modeling and Simulations*. John Wiley & Sons, 2012, pp. 407-416

52. Danaei, Goodarz, et al. "National, Regional, and Global Trends in Fasting Plasma Glucose and Diabetes Prevalence since 1980: Systematic Analysis of Health Examination Surveys and Epidemiological Studies with 370 Country-Years and 2·7 Million Participants." The Lancet, vol. 378, no. 9785, 25 June 2011, pp. 31–40., doi:10.1016/s0140-6736(11)60679-x.

Appendix

APPENDIX I Differential Equations for ODE Compartmental Analysis

Collapsed Terms

$$k_{tot\ liv_i} = k_{liv_i} * y_{liv} + k_{int_o} * y_{int} + k_{vat_o} * y_{vat} + k_{pan_o} * y_{pan}$$

Glucose Compartments

$$\frac{dy_{cir\ g}}{dt} = -k_{cir_o} * y_{cir\ g} + k_{liv_o} * y_{liv\ g} + k_{mus_o} * y_{mus\ g} - k_{eli\ g} * y_{cir\ g}$$

$$\frac{dy_{int\ g}}{dt} = k_{int_i} * y_{cir\ g} - \left(k_{int_o} + k_{per_o} + k_{eli\ g}\right) * y_{int\ g} + k_{dis} * y_{food}$$

$$\frac{dy_{vat\ g}}{dt} = k_{vat_i} * y_{cir\ g} - \left(k_{vat_o} + k_{eli\ g} - k_{ins\ cons\ g} * f_{vat\ i}\right) * y_{vat\ g} + k_{per_o} * y_{int\ g}$$

$$\frac{dy_{pan\ g}}{dt} = k_{pan_i} * y_{cir\ g} - \left(k_{pan_o} + k_{eli\ g}\right) * y_{pan\ g}$$

$$\frac{dy_{liv\ g}}{dt} = k_{tot\ liv_i\ g} - \left(k_{liv_o} + k_{eli\ g} + k_{ins\ cons\ g} * f_{liv\ i}\right) * y_{liv\ g} + f_{liv\ l} * k_{liv\ gen}$$

$$\frac{dy_{mus\ g}}{dt} = k_{mus_i} * y_{cir\ g} - \left(k_{mus_o} + k_{eli\ g} - k_{ins\ cons\ g} * f_{mus\ i}\right) * y_{mus\ g}$$

$$-k_{dis} * y_{food}$$

Glucagon Compartments

$$\frac{dy_{cir\ l}}{dt} = -k_{cir_o} * y_{cir\ l} + k_{liv_o} * y_{liv\ l} + k_{mus_o} * y_{mus\ l} - k_{eli\ g} * y_{cir\ l}$$

$$\frac{dy_{int\ l}}{dt} = k_{int_i} * y_{cir\ l} - \left(k_{int_o} + k_{per_o}\right) * y_{int\ l}$$

$$\frac{dy_{vat\ l}}{dt} = k_{vat_i} * y_{cir\ l} - k_{vat_o} * y_{vat\ l} + k_{per_o} * y_{int\ l}$$

$$\frac{dy_{pan\ l}}{dt} = k_{pan_i} * y_{cir\ l} - k_{pan_o} * y_{pan\ l} + k_{gen\ l} * I_{pan\ l}$$

$$\frac{dy_{liv\ l}}{dt} = k_{tot\ liv_i\ l} - \left(k_{liv_o} + k_{eli\ l}\right) * y_{liv\ l}$$

$$\frac{dy_{mus\ l}}{dt} = k_{mus_i} * y_{cir\ l} - k_{mus_o} * y_{mus\ l}$$

Insulin Compartments

$$\frac{dy_{cir\,i}}{dt} = -k_{cir_o} * y_{cir\,i} + k_{liv_o} * y_{liv\,i} + k_{mus_o} * y_{mus\,i} - k_{eli\,i} * y_{cir\,i}$$

$$\frac{dy_{int\,i}}{dt} = k_{int_i} * y_{cir\,i} - \left(k_{int_o} + k_{per_o}\right) * y_{int\,i}$$

$$\frac{dy_{vat\,i}}{dt} = k_{vat_i} * y_{cir\,i} - \left(k_{vat_o} + k_{eli\,i}\right) * y_{vat\,i} + k_{per_o} * y_{int\,i}$$

$$\frac{dy_{pan\,i}}{dt} = k_{pan_i} * y_{cir\,i} - k_{pan_o} * y_{pan\,i} + S_{pan\,i} * k_{gen\,i}$$

$$\frac{dy_{liv\,i}}{dt} = k_{tot\,liv_i\,i} - \left(k_{liv_o} + k_{eli\,i}\right) * y_{liv\,i}$$

$$\frac{dy_{mus\,i}}{dt} = k_{mus_i} * y_{cir\,i} - \left(k_{mus_o} + k_{eli\,i}\right) * y_{mus\,i}$$

Non Glycated Beta Amyloids

$$\frac{dy_{cir\,b}}{dt} = -k_{cir_o} * y_{cir\,b} + k_{liv_o} * y_{liv\,b} + k_{mus_o} * y_{mus\,b} - k_{eli\,b} * f_{cir\,b} + k_{gen\,b} - \frac{k_{rxn} * y_{cir\,g} * y_{cir\,b}}{V_{cir}}$$

$$\frac{dy_{int\,b}}{dt} = k_{int_i} * y_{cir\,b} - \left(k_{int_o} + k_{per_o}\right) * y_{int\,b} + \frac{k_{gen\,b}}{2} - k_{eli\,b} * f_{int\,b} - \frac{k_{rxn} * y_{int\,g} * y_{int\,b}}{V_{int}}$$

$$\frac{dy_{vat\,b}}{dt} = k_{vat_i} * y_{cir\,b} - k_{vat_o} * y_{vat\,b} + k_{per_o} * y_{int\,b} - \frac{k_{rxn} * y_{cir\,g} * y_{int\,b}}{V_{int}}$$

$$\frac{dy_{pan\,b}}{dt} = k_{pan_i} * y_{cir\,b} - k_{pan_o} * y_{pan\,b} + \frac{k_{gen\,b}}{2} - \frac{k_{rxn} * y_{pan\,g} * y_{pan\,b}}{V_{pan}}$$

$$\frac{dy_{liv\,b}}{dt} = k_{tot\,liv_i\,b} - k_{liv_o} * y_{liv\,b} - k_{eli\,b} * f_{liv\,b} - \frac{k_{rxn} * y_{liv\,g} * y_{liv\,b}}{V_{liv}}$$

$$\frac{dy_{mus\,b}}{dt} = k_{mus_i} * y_{cir\,b} - k_{mus_o} * y_{mus\,b} - \frac{k_{rxn} * y_{mus\,g} * y_{mus\,b}}{V_{mus}}$$

Glycated Beta Amyloids

$$\frac{dy_{cir\,bg}}{dt} = -k_{cir_o} * y_{cir\,b} + k_{liv_o} * y_{liv\,bg} + k_{mus_o} * y_{mus\,bg} - k_{eli\,bg} * f_{cir\,bg} + \frac{k_{rxn} * y_{cir\,g} * y_{cir\,b}}{V_{cir}}$$

$$\frac{dy_{int\,bg}}{dt} = k_{int_i} * y_{cir\,bg} - \left(k_{int_o} + k_{per_o}\right) * y_{int\,bg} - k_{eli\,bg} * f_{int\,bg} + \frac{k_{rxn} * y_{int\,g} * y_{int\,b}}{V_{int}}$$

$$\frac{dy_{vat\,bg}}{dt} = k_{vat_i} * y_{cir\,bg} - k_{vat_o} * y_{vat\,bg} + k_{per_o} * y_{int\,bg} + \frac{k_{rxn} * y_{cir\,g} * y_{int\,b}}{V_{int}}$$

$$\frac{dy_{pan\,bg}}{dt} = k_{pan_i} * y_{cir\,bg} - k_{pan_o} * y_{pan\,bg} + \frac{k_{rxn} * y_{pan\,g} * y_{pan\,b}}{V_{pan}}$$

$$\frac{dy_{liv\,bg}}{dt} = k_{tot\,liv_i\,bg} - k_{liv_o} * y_{liv\,bg} - k_{eli\,bg} * f_{liv\,bg} + \frac{k_{rxn} * y_{liv\,g} * y_{liv\,b}}{V_{liv}}$$

$$\frac{dy_{mus\,bg}}{dt} = k_{mus_i} * y_{cir\,bg} - k_{mus_o} * y_{mus\,bg} + \frac{k_{rxn} * y_{mus\,g} * y_{mus\,b}}{V_{mus}}$$

Fractional Bound Terms

$$S_{pan\,i} = 1 + E_{\max pan\,i} * \frac{C_{pan\,g} - u_{pan\,g}}{\left(EC50_i - u_{pan\,g}\right) + \left(C_{pan\,g} - u_{pan\,g}\right)} H(C_{pan\,g})$$

$$I_{pan\,l} = 1 - E_{\min pan\,l} * \frac{C_{pan\,i} - m_{pan\,i}}{\left(IC50_l - m_{pan\,i}\right) + \left(C_{pan\,i} - m_{pan\,i}\right)} H(C_{pan\,i})$$

$$f_{org\,h} = \frac{E_{\max h} * C_{org\,h\,dif}}{(k_{D_h} - C_{org\,h\,base}) + C_{org\,h\,dif}}$$

y: Mass of a species

$z_{a\,c\,b}$: a (Compartment) , b (In or Out of Compartment), c(Species)

g – glucose, l – glucagon, i – insulin, b – Aβ, bg – glycated Aβ

k_{per} : Perfusion of leaked species from intestines to VAT

k_{dis}: Glucose absorption rate from food into intestines

k_{eli}: Elimination rate constant

$k_{liv\,gen}$: Glucose generation in liver due to glycogenolysis

$k_{ins\,cons\,g}$: Insulin mediated glucose elimination rate constant

$k_{gen\,l}$: Glucagon generation rate from pancreas

$k_{gen\,i}$: Insulin generation rate from pancreas

$k_{gen\,b}$: Aβ generation rate

k_{rxn}: 2nd order glycation reaction rate

E_{max}: Maximum effect constant

$H(C)$: Step function of concentration parameter

$$H(C > C_{threshold}) = 1$$

$$H(C \leq C_{threshold}) = 0$$

C_{dif}: Difference of concentration with baseline concentration in a compartment

$f_{org\,h}$: Fractional bound term. org – Compartment, h - species

APPENDIX 2 ODE PARAMETERS

Organ Volume	Volume (dL)	Blood Flow Rate (dL/hr)	Rate Constant k_in (1/hr)	Rate Constant k_out (1/hr)
Circulatory System	4.87	~	~	~
Intestines	11.2	54600	11211	4875
VAT	0.3	270	55	900
Pancreas	1.11	7980	1639	7189
Liver	25.1	88200	18111	3514
Muscle	7.43	44940	9228	6048

Table 1[51]: Volume, Blood Flows, and Rate Constants of Organs

Blood Compartment Concentrations	Glucose (mg/dL)	Glucagon (mg/dL)	Insulin (mg/dL)	Aβ (mg/dL)	Aβ Glycated (mg/dL)
Circulatory System	84.9	1.53E-08	2.90E-05	1.39E-06	2.08E-09
Intestines	84.9	1.53E-08	2.90E-05	1.39E-06	2.08E-09
VAT	84.8	1.53E-08	2.90E-05	1.39E-06	2.09E-09
Pancreas	84.9	1.55E-08	2.92E-05	1.40E-06	2.08E-09
Liver	84.9	1.53E-08	2.90E-05	1.39E-06	2.08E-09
Skeletal Muscle	84.9	1.53E-08	2.90E-05	1.39E-06	2.08E-09

Table 2[49, 50, 52]: Baseline Concentrations of Compartments for each Species

Elimination Constants	Units (1/hr)
$k_{eli\ g}$	1.7
$k_{eli\ l}$	1.5
$k_{eli\ i}$	10
$k_{eli\ b}$	123.15
$k_{eli\ bg}$	123.15

Table 3: Elimination Rate Constants for each Species

Generation Constants	Units (mg/hr)
$k_{liv\ gen}$	7.36E+03
$k_{gen\ l}$	1.50E-06
$k_{gen\ i}$	0.0016

$k_{gen\ b}$	8.19E-05

Table 4: Generation Rate Constants for each Species

Dissociation Constants	Units (mg/dL)
k_D_g_gen	8.71E-04
k_D_i_cons	3.18E-05
k_D_b	3.14
k_D_bg	4.71

Table 5: Dissociation Constants for each Species to Respective Receptors/Proteins

Effect Constants	Values	Units
$EC50_i$	300	mg/dL
$E_{max\ pan\ i}$	50	~
$IC50_I$	8.71E-04	mg/dL
$E_{min\ pan\ I}$	2	~
$E_{max\ cons}$	31	~

Table 6: Effect Modeling Compartments Used for Secretion of Hormones and Insulin Action

APPENDIX 3 MATLAB Code of Compartmental Model Script

```
%{
This model accounts for insulin and glucagon in response to glucose changes
in the blood to mediate a healthy glucose response in an adult 70kg male.
Using the glucose concentrations in the compartments, we quantify its
effect on beta amyloid accumulation in the compartments.
%}
Global Variables
global t_fin;
global Ab_stab;
global iv_1;
Volume Parameters for Concentrations
V_vat_bl = 2.97 / 10 ;
V_liv_bl = 25.1 ;
V_mus_bl = 7.43 ;
V_int_bl = 11.2 ;
V_pan_bl = 15.8/100*70/10;
V_cir = (50 - (V_vat_bl + V_liv_bl + V_mus_bl + V_int_bl + V_pan_bl));
V_arr = [V_cir V_int_bl V_vat_bl V_pan_bl V_liv_bl V_mus_bl];
Initial Values for each Species and Dose
dose1 = 50000;
dose2 = 5000;
m_lvl_g = 85;
m_lvl_i = 0.00002904;
m_lvl_l = 1.532388 * (10 ^ (-8));
m_lvl_b = (14.33*(10^(-9))) / 0.01;
m_lvl_bg = 0.03 * m_lvl_b;
m_lvl_b = m_lvl_b * 0.97;
```

```
iv_1 = [
    m_lvl_g*V_cir;          %Glucose
    m_lvl_g*V_int_bl;
    m_lvl_g*V_vat_bl;
    m_lvl_g*V_pan_bl;
    m_lvl_g*V_liv_bl;
    m_lvl_g*V_mus_bl;

    m_lvl_l*V_cir;          %Glucagon
    m_lvl_l*V_int_bl;
    m_lvl_l*V_vat_bl;
    m_lvl_l*V_pan_bl;
    m_lvl_l*V_liv_bl;
    m_lvl_l*V_mus_bl;

    m_lvl_i*V_cir;          %Insulin
    m_lvl_i*V_int_bl;
    m_lvl_i*V_vat_bl;
    m_lvl_i*V_pan_bl;
    m_lvl_i*V_liv_bl;
    m_lvl_i*V_mus_bl;

    m_lvl_b*V_cir;          %Beta Amyloid
    m_lvl_b*V_int_bl;
    m_lvl_b*V_vat_bl;
    m_lvl_b*V_pan_bl;
    m_lvl_b*V_liv_bl;
    m_lvl_b*V_mus_bl;
```

```
    m_lvl_bg*V_cir;             %Glycated Beta Amyloid
    m_lvl_bg*V_int_bl;
    m_lvl_bg*V_vat_bl;
    m_lvl_bg*V_pan_bl;
    m_lvl_bg*V_liv_bl;
    m_lvl_bg*V_mus_bl;

    0;          %Food
    ];
ODE Solver
t_ini = 0;
t_fin = 5;
tspan = t_ini:0.1:t_fin;
[t, Ab] = ode15s(@ModelPB_G_I_L_BA, tspan, iv_1); %Sets up system
t_stab = t;
Ab_stab = Ab(end, :);

initial_values = Ab_stab;
init_vol_ar = initial_values(7:end);
initial_values(end) = initial_values(end) + dose1;

t_add = 4;
t_end = t_fin + t_add;
tspan = [t_fin t_end];
[t, Ab] = ode15s(@ModelPB_G_I_L_BA, tspan, initial_values);
Ab = [Ab; Ab];
t = [t; t];
```

Concentration Calculations

%Glucose

```
Ab_cir_g = Ab(:,1);
Ab_int_g = Ab(:,2);
Ab_vat_g = Ab(:,3);
Ab_pan_g = Ab(:,4);
Ab_liv_g = Ab(:,5);
Ab_mus_g = Ab(:,6);
Cp_cir_g = Ab_cir_g / V_cir;
Cp_int_g = Ab_int_g / V_int_bl;
Cp_vat_g = Ab_vat_g / V_vat_bl;
Cp_pan_g = Ab_pan_g / V_pan_bl;
Cp_liv_g = Ab_liv_g / V_liv_bl;
Cp_mus_g = Ab_mus_g / V_mus_bl;
```

%Glucagon

```
Ab_cir_l = Ab(:,7);
Ab_int_l = Ab(:,8);
Ab_vat_l = Ab(:,9);
Ab_pan_l = Ab(:,10);
Ab_liv_l = Ab(:,11);
Ab_mus_l = Ab(:,12);
Cp_cir_l = Ab_cir_l / V_cir;
Cp_int_l = Ab_int_l / V_int_bl;
Cp_vat_l = Ab_vat_l / V_vat_bl;
Cp_pan_l = Ab_pan_l / V_pan_bl;
Cp_liv_l = Ab_liv_l / V_liv_bl;
Cp_mus_l = Ab_mus_l / V_mus_bl;
```

```
Cp_cir_l_f = Ab_cir_l / init_vol_ar(1);
Cp_int_l_f = Ab_int_l / init_vol_ar(2);
Cp_vat_l_f = Ab_vat_l / init_vol_ar(3);
Cp_pan_l_f = Ab_pan_l / init_vol_ar(4);
Cp_liv_l_f = Ab_liv_l / init_vol_ar(5);
Cp_mus_l_f = Ab_mus_l / init_vol_ar(6);

%Insulin
Ab_cir_i = Ab(:,13);
Ab_int_i = Ab(:,14);
Ab_vat_i = Ab(:,15);
Ab_pan_i = Ab(:,16);
Ab_liv_i = Ab(:,17);
Ab_mus_i = Ab(:,18);
Cp_cir_i = Ab_cir_i / V_cir;
Cp_int_i = Ab_int_i / V_int_bl;
Cp_vat_i = Ab_vat_i / V_vat_bl;
Cp_pan_i = Ab_pan_i / V_pan_bl;
Cp_liv_i = Ab_liv_i / V_liv_bl;
Cp_mus_i = Ab_mus_i / V_mus_bl;
Cp_cir_i_f = Ab_cir_i / init_vol_ar(7);
Cp_int_i_f = Ab_int_i / init_vol_ar(8);
Cp_vat_i_f = Ab_vat_i / init_vol_ar(9);
Cp_pan_i_f = Ab_pan_i / init_vol_ar(10);
Cp_liv_i_f = Ab_liv_i / init_vol_ar(11);
Cp_mus_i_f = Ab_mus_i / init_vol_ar(12);

%Beta Amyloid 1-42 Unglycated
```

```
Ab_cir_b = Ab(:,19);
Ab_int_b = Ab(:,20);
Ab_vat_b = Ab(:,21);
Ab_pan_b = Ab(:,22);
Ab_liv_b = Ab(:,23);
Ab_mus_b = Ab(:,24);
Cp_cir_b = Ab_cir_b / V_cir;
Cp_int_b = Ab_int_b / V_int_bl;
Cp_vat_b = Ab_vat_b / V_vat_bl;
Cp_pan_b = Ab_pan_b / V_pan_bl;
Cp_liv_b = Ab_liv_b / V_liv_bl;
Cp_mus_b = Ab_mus_b / V_mus_bl;
Cp_cir_b_f = Ab_cir_b / init_vol_ar(13);
Cp_int_b_f = Ab_int_b / init_vol_ar(14);
Cp_vat_b_f = Ab_vat_b / init_vol_ar(15);
Cp_pan_b_f = Ab_pan_b / init_vol_ar(16);
Cp_liv_b_f = Ab_liv_b / init_vol_ar(17);
Cp_mus_b_f = Ab_mus_b / init_vol_ar(18);

%Beta Amyloid 1-42 Glycated
Ab_cir_bg = Ab(:,25);
Ab_int_bg = Ab(:,26);
Ab_vat_bg = Ab(:,27);
Ab_pan_bg = Ab(:,28);
Ab_liv_bg = Ab(:,29);
Ab_mus_bg = Ab(:,30);
Cp_cir_bg = Ab_cir_bg / V_cir;
Cp_int_bg = Ab_int_bg / V_int_bl;
```

```
Cp_vat_bg = Ab_vat_bg / V_vat_bl;
Cp_pan_bg = Ab_pan_bg / V_pan_bl;
Cp_liv_bg = Ab_liv_bg / V_liv_bl;
Cp_mus_bg = Ab_mus_bg / V_mus_bl;
Cp_cir_bg_f = Ab_cir_bg / init_vol_ar(19);
Cp_int_bg_f = Ab_int_bg / init_vol_ar(20);
Cp_vat_bg_f = Ab_vat_bg / init_vol_ar(21);
Cp_pan_bg_f = Ab_pan_bg / init_vol_ar(22);
Cp_liv_bg_f = Ab_liv_bg / init_vol_ar(23);
Cp_mus_bg_f = Ab_mus_bg / init_vol_ar(24);
```

APPENDIX IV MATLAB Code of Compartmental Model ODE System

```
%{
Glucose homeostasis multi compartment model ODE to quantify beta amyloid
accumulation due to glucose concentrations in compartments
%}

function [dydt] = ModelPB_G_I_L_BA(t,y)
Global Variables
global t_fin;
global Ab_stab;
global iv_1;
Organ & Blood Flow Constants
V_vat_bl = 2.97 / 10;
V_liv_bl = 25.1;
V_mus_bl = 7.43;
V_int_bl = 11.2;
V_pan_bl = 15.8/100*70/10;
V_cir = (50 - (V_vat_bl + V_liv_bl + V_mus_bl + V_int_bl + V_pan_bl));

u_lvl_g = 110;
if (t <= t_fin)
   i_v = iv_1;
else
   i_v = Ab_stab(end, :);
end

Q_vat = 270;
Q_mus = 749 * 60;
```

```
Q_int = 910 * 60;
Q_pan = 133 * 60;
Q_liv = 1470 * 60;
Q_per = (185*1000./24)./(85*V_vat_bl); %Perfusion from Int to VAT

k_per_o = Q_per ./ V_int_bl;
k_int_o = Q_int ./ V_int_bl;
k_vat_o = (Q_vat + Q_per) ./ V_vat_bl;
k_pan_o = Q_pan ./ V_pan_bl;
k_liv_o = (Q_liv + Q_int + Q_pan + Q_vat + Q_per) ./ V_liv_bl;
k_mus_o = Q_mus ./ V_mus_bl;

k_int_i = (Q_int + Q_per) ./ V_cir;
k_vat_i = Q_vat ./ V_cir;
k_liv_i = Q_liv ./ V_cir;
k_mus_i = Q_mus ./ V_cir;
k_pan_i = Q_pan ./ V_cir;
Food Glucose Absorption/Elimination and Hormone Constants
%Glucose Constants
k_eli_g = 1.7;
k_dis = 0.5; %Absorption Constant of glucose

%Insulin Constants
k_eli_i = 1.7;
EC50_i = 300; %Response to generate insulin in pancreas %VC

%Glucagon Constants
k_eli_l = 3;
```

```
f_nM_mg_dL = 1 ./ (10^9) * 3482.7 * 1000 ./ 10;
k_D_g_gen = 2.5*f_nM_mg_dL; %Response of glucagon on liver
EC50_l = k_D_g_gen; %Response to generate glucagon in pancreas

%Concentrations in compartments
C_liv_l = y(11) ./ V_liv_bl;
C_liv_l_c = i_v(11) ./ V_liv_bl;
C_pan_i = y(16) ./ V_pan_bl;
C_pan_g = y(4) ./ V_pan_bl;
C_pan_i_c = i_v(16) ./ V_pan_bl;
C_pan_g_du = C_pan_g - u_lvl_g;
C_pan_i_dm = C_pan_i - C_pan_i_c;

if (C_pan_g_du < 0)
   C_pan_g_du = 0;
end
if (C_pan_i_dm < 0)
   C_pan_i_dm = 0;
end

%Effect Compartments
E_max_pan_i = 50;
E_min_pan_l = 2;
I_pan_l = 1 - E_min_pan_l * C_pan_i_dm ./ ((EC50_l - C_pan_i_c) + C_pan_i_dm);
I_pan_l_c = 1;
hc = 1;
S_pan_i = 1 + E_max_pan_i * (C_pan_g_du^hc) ./ ((EC50_i - u_lvl_g)^hc + C_pan_g_du^hc);
```

```
dif_liv_l = abs(C_liv_l - C_liv_l_c);
f_liv_l_c = 1;
EC50_l_liv = C_liv_l_c * 10 - C_liv_l_c;
if (C_liv_l >= C_liv_l_c)
   f_liv_l = f_liv_l_c + dif_liv_l ./ (EC50_l_liv + dif_liv_l);
else
   f_liv_l = f_liv_l_c - dif_liv_l ./ (EC50_l_liv + dif_liv_l);
end
Insulin Enhanced glucose absorption
C_mus_i = y(18) ./ V_mus_bl;
C_mus_i_c = i_v(18) ./ V_mus_bl;
C_vat_i = y(15) ./ V_vat_bl;
C_vat_i_c = i_v(15) ./ V_vat_bl;
C_liv_i = y(17) ./ V_liv_bl;
C_liv_i_c = i_v(17) ./ V_liv_bl;

%Insulin Consumption Effect
k_ins_g_cons = 0.1;
k_D_i_cons = (3.7 / (10^9) * 5734 / 10)*15; %Response to consume glucose from insulin
E_max_cons = 31;%30;
dif_mus = C_mus_i - C_mus_i_c;
dif_vat = C_vat_i - C_vat_i_c;
dif_liv = C_liv_i - C_liv_i_c;

if (dif_mus < 0)
   dif_mus = 0;
end
if (dif_vat < 0)
```

```
   dif_vat = 0;
end
if (dif_liv < 0)
   dif_liv = 0;
end


hc_i = 1;
f_mus_i_c = C_mus_i / (k_D_i_cons + C_mus_i);
f_vat_i_c = C_vat_i / (k_D_i_cons + C_vat_i);
f_liv_i_c = C_liv_i / (k_D_i_cons + C_liv_i);
f_mus_i = f_mus_i_c + E_max_cons * (dif_mus^hc_i) ./ ((k_D_i_cons-C_mus_i_c)^hc_i +
dif_mus^hc_i);
f_vat_i = f_vat_i_c + E_max_cons * (dif_vat^hc_i) ./ ((k_D_i_cons-C_vat_i_c)^hc_i +
dif_vat^hc_i);
f_liv_i = f_liv_i_c + E_max_cons * (dif_liv^hc_i) ./ ((k_D_i_cons-C_liv_i_c)^hc_i +
dif_liv^hc_i);
Generation Constants
k_liv_gen = (k_eli_g*sum(i_v(1:6)) + k_ins_g_cons*(f_vat_i_c*i_v(3) + f_liv_i_c*i_v(5) +
f_mus_i_c*i_v(6))) ./ f_liv_l_c;
k_gen_l = k_eli_l * (i_v(11) + i_v(12)) ./ I_pan_l_c;
k_gen_i = k_eli_i * (i_v(15) + i_v(17) + i_v(18));
Beta Amyloid Protein Binding Elimination
fac = 1.5;
k_D_b = (6.95 * (10 ^(-6)) * 4514.04 ./ 10 * 1000);
k_D_bg = k_D_b * fac;


%Competitive Protein Binding with NEP betw Glycated and Non-Glycated BA
C_cir_b = y(19) ./ V_cir;
C_int_b = y(20) ./ V_int_bl;
C_liv_b = y(23) ./ V_liv_bl;
```

```
C_cir_bg = y(25) ./ V_cir;
C_int_bg = y(26) ./ V_int_bl;
C_liv_bg = y(29) ./ V_liv_bl;

f_cir_b = C_cir_b ./ (C_cir_b + k_D_b * (1 + (C_cir_bg ./ k_D_bg)));
f_int_b = C_int_b ./ (C_int_b + k_D_b * (1 + (C_int_bg ./ k_D_bg)));
f_liv_b = C_liv_b ./ (C_liv_b + k_D_b * (1 + (C_liv_bg ./ k_D_bg)));

f_cir_bg = C_cir_bg ./ (C_cir_bg + k_D_bg * (1 + (C_cir_b ./ k_D_b)));
f_int_bg = C_int_bg ./ (C_int_bg + k_D_bg * (1 + (C_int_b ./ k_D_b)));
f_liv_bg = C_liv_bg ./ (C_liv_bg + k_D_bg * (1 + (C_liv_b ./ k_D_b)));

i_cir_c = i_v(19) ./ V_cir;
i_int_c = i_v(20) ./ V_int_bl;
i_liv_c = i_v(23) ./ V_liv_bl;
i_cir_cg = i_v(25) ./ V_cir;
i_int_cg = i_v(26) ./ V_int_bl;
i_liv_cg = i_v(29) ./ V_liv_bl;

f_cir_c = i_cir_c ./ (i_cir_c + k_D_b * (1 + (i_cir_cg ./ k_D_bg)));
f_int_c = i_int_c ./ (i_int_c + k_D_b * (1 + (i_int_cg ./ k_D_bg)));
f_liv_c = i_liv_c ./ (i_liv_c + k_D_b * (1 + (i_liv_cg ./ k_D_bg)));

k_eli_b = 123.15;
k_eli_bg = k_eli_b;

beta =  (i_v(1)*i_v(19)./V_cir + i_v(2)*i_v(20)./V_int_bl + i_v(3)*i_v(21)./V_vat_bl +
i_v(4)*i_v(22)./V_pan_bl + i_v(5)*i_v(23)./V_liv_bl + i_v(6)*i_v(24)./V_mus_bl);
```

k_{rxn} = 0.23 / 85 * 0.1;

k_gen_b = 0.5 * (k_eli_b * (f_cir_c + f_int_c + f_liv_c) + (k_{rxn} * beta));

Accumulation of Beta Amyloids in plasma

Age - 34 -> 64 yrs plasma BA 1-42 - 14.33 -> 18.54 frac change (a) - (18.54 - 14.33) / 14.33 slope - (a)/(64-34)/365 (frac change / days) slope - (a)/(64-34)/365/24 (frac change / hrs)

```
if (t > t_fin)
    frac_change = (18.54 - 14.33) / 14.33;
    rate_accum = frac_change / (30 * 365 * 24);
    rate_degrd = 1 - rate_accum * t*0.78888888;
    k_eli_b = k_eli_b * rate_degrd;
    k_eli_bg = k_eli_b;
end
```

Collapsed Constants

```
k_cir_o = k_int_i + k_vat_i + k_liv_i + k_mus_i + k_pan_i;
k_liv_g_i_tot = (k_liv_i * y(1)) + (k_int_o * y(2)) + (k_vat_o * y(3)) + (k_pan_o * y(4));
k_liv_l_i_tot = (k_liv_i * y(7)) + (k_int_o * y(8)) + (k_vat_o * y(9)) + (k_pan_o * y(10));
k_liv_i_i_tot = (k_liv_i * y(13)) + (k_int_o * y(14)) + (k_vat_o * y(15)) + (k_pan_o * y(16));
k_liv_b_i_tot = (k_liv_i * y(19)) + (k_int_o * y(20)) + (k_vat_o * y(21)) + (k_pan_o * y(22));
k_liv_bg_i_tot = (k_liv_i * y(25)) + (k_int_o * y(26)) + (k_vat_o * y(27)) + (k_pan_o * y(28));
```

SOE

```
dydt = [

    %GLUCOSE - Blood
    %1-Circulatory Blood
    -k_cir_o * y(1) + k_liv_o * y(5) + k_mus_o * y(6) - k_eli_g * y(1);
    %2-Intestines
    k_int_i * y(1) - (k_int_o + k_per_o) * y(2) - k_eli_g * y(2) + k_dis * y(end);
    %3-Visceral Adipose Tissue (VAT)
    k_vat_i * y(1) - k_vat_o * y(3) - k_eli_g * y(3) + k_per_o * y(2) - k_ins_g_cons * f_vat_i *
y(3);
```

```
%4-Pancreas
k_pan_i * y(1) - k_pan_o * y(4) - k_eli_g * y(4);
%5-Liver
k_liv_g_i_tot - k_liv_o * y(5) - k_eli_g * y(5) + f_liv_l*k_liv_gen - k_ins_g_cons * f_liv_i *
y(5);
%6-Muscle
k_mus_i * y(1) - k_mus_o * y(6) - k_eli_g * y(6) - k_ins_g_cons * f_mus_i * y(6);

%GLUCAGON
%7-Circulatory Blood
-k_cir_o * y(7) + k_liv_o * y(11) + k_mus_o * y(12);
%8-Intestines
k_int_i * y(7) - (k_int_o) * y(8) - k_per_o * y(8);
%9-Visceral Adipose Tissue (VAT)
k_vat_i * y(7) - (k_vat_o) * y(9) + k_per_o * y(8);
%10-Pancreas
k_pan_i * y(7) - (k_pan_o) * y(10) + k_gen_l * I_pan_l;
%11-Liver
k_liv_l_i_tot  - k_liv_o * y(11) - k_eli_l * y(11);
%12-Muscle
k_mus_i * y(7) - (k_mus_o + k_eli_l) * y(12);

%INSULIN
%13-Circulatory Blood
-k_cir_o * y(13) + k_liv_o * y(17) + k_mus_o * y(18);
%14-Intestines
k_int_i * y(13) - (k_int_o) * y(14) - k_per_o * y(14);
%15-Visceral Adipose Tissue (VAT)
k_vat_i * y(13) - (k_vat_o + k_eli_i) * y(15) + k_per_o * y(14);
```

%16-Pancreas

k_pan_i * y(13) - (k_pan_o) * y(16) + k_gen_i * S_pan_i;

%17-Liver

k_liv_i_i_tot - (k_liv_o + k_eli_i) * y(17);

%18-Muscle

k_mus_i * y(13) - (k_mus_o + k_eli_i) * y(18);

%BETA AMYLOID

%19-Circulatory Blood

-k_cir_o * y(19) + k_liv_o * y(23) + k_mus_o * y(24) - k_eli_b * f_cir_b + k_gen_b - k_{rxn} * y(1) * y(19) / (V_cir^1);

%20-Intestines

k_int_i * y(19) - (k_int_o + k_per_o) * y(20) - k_eli_b * f_int_b + k_gen_b/2 - k_{rxn} * y(2) * y(20) / (V_int_bl^1);

%21-Visceral Adipose Tissue (VAT)

k_vat_i * y(19) + k_per_o * y(20) - k_vat_o * y(21) - k_{rxn} * y(3) * y(21) / (V_vat_bl^1);

%22-Pancreas

k_pan_i * y(19) - k_pan_o * y(22) + k_gen_b/2 - k_{rxn} * y(4) * y(22) / (V_pan_bl^1);

%23-Liver

k_liv_b_i_tot - k_liv_o * y(23) - k_eli_b * f_liv_b - k_{rxn} * y(5) * y(23) / (V_liv_bl^1);

%24-Muscle

k_mus_i * y(19) - k_mus_o * y(24) - k_{rxn} * y(6) * y(24) / (V_mus_bl^1);

%GLYCATED - BETA AMYLOID

%25-Circulatory Blood

-k_cir_o * y(25) + k_liv_o * y(29) + k_mus_o * y(30) - k_eli_bg * f_cir_bg + k_{rxn} * y(1) * y(19) / (V_cir^1);

%26-Intestines

k_int_i * y(25) - (k_int_o + k_per_o) * y(26) - k_eli_bg * f_int_bg + k_{rxn} * y(2) * y(20) / (V_int_bl^1);

```
    %27-Visceral Adipose Tissue (VAT)
    k_vat_i * y(25) + k_per_o * y(26) - k_vat_o * y(27)  + k_rxn * y(3) * y(21) / (V_vat_bl^1);
    %28-Pancreas
    k_pan_i * y(25) - k_pan_o * y(28) + k_rxn * y(4) * y(22) / (V_pan_bl^1);
    %29-Liver
    k_liv_bg_i_tot - k_liv_o * y(29) - k_eli_bg * f_liv_bg + k_rxn * y(5) * y(23) / (V_liv_bl^1);
    %30-Muscle
    k_mus_i * y(25) - k_mus_o * y(30) + k_rxn * y(6) * y(24) / (V_mus_bl^1);

    %31-Food
    (-k_dis * y(end));
    ];
end
```

APPENDIX V MATLAB Code for Repeated Meals w/ Variable Factor

```
dose = 50000;

V_vat_bl = 2.97 / 10 ;
V_liv_bl = 25.1 ;
V_mus_bl = 7.43 ;
V_int_bl = 11.2 ;
V_pan_bl = 15.8/100*70/10;
V_cir = (50 - (V_vat_bl + V_liv_bl + V_mus_bl + V_int_bl + V_pan_bl));
V_arr = [V_cir V_int_bl V_vat_bl V_pan_bl V_liv_bl V_mus_bl];

m_lvl_g = 85;
m_lvl_i = 0.00002904;
m_lvl_l = 1.532388 * (10 ^ (-8));
m_lvl_b = (14.33*(10^(-9))) / 0.01;
m_lvl_bg = 0.03 * m_lvl_b;
m_lvl_b = m_lvl_b * 0.97;
iv_1 = [
   m_lvl_g*V_cir;            %Glucose
   m_lvl_g*V_int_bl;
   m_lvl_g*V_vat_bl;
   m_lvl_g*V_pan_bl;
   m_lvl_g*V_liv_bl;
   m_lvl_g*V_mus_bl;

   m_lvl_l*V_cir;            %Glucagon
   m_lvl_l*V_int_bl;
   m_lvl_l*V_vat_bl;
```

```
m_lvl_l*V_pan_bl;
m_lvl_l*V_liv_bl;
m_lvl_l*V_mus_bl;

m_lvl_i*V_cir;          %Insulin
m_lvl_i*V_int_bl;
m_lvl_i*V_vat_bl;
m_lvl_i*V_pan_bl;
m_lvl_i*V_liv_bl;
m_lvl_i*V_mus_bl;

m_lvl_b*V_cir;          %Beta Amyloid
m_lvl_b*V_int_bl;
m_lvl_b*V_vat_bl;
m_lvl_b*V_pan_bl;
m_lvl_b*V_liv_bl;
m_lvl_b*V_mus_bl;

m_lvl_bg*V_cir;         %Glycated Beta Amyloid
m_lvl_bg*V_int_bl;
m_lvl_bg*V_vat_bl;
m_lvl_bg*V_pan_bl;
m_lvl_bg*V_liv_bl;
m_lvl_bg*V_mus_bl;

0;      %Food
];
```

```
global t_fin;
global Ab_stab;
global k_fac;

ba_bag_range = 19:(length(iv_1)-1);
reset_ba_bag = iv_1(ba_bag_range);

k_fac_var = [0.1 0.2 0.5 1 2 5 10];
k1 = 0;
k2 = 0;
k3 = 0;
k4 = 0;
k5 = 0;
k6 = 0;
k7 = 0;
t1 = 0;
t2 = 0;
t3 = 0;
t4 = 0;
t5 = 0;
t6 = 0;
t7 = 0;


for rp_fac = 1:length(k_fac_var)
    k_fac = k_fac_var(rp_fac);
    t_ini = 0;
    t_fin = 5;
```

```
    tspan = t_ini:0.1:t_fin;
    [t, Ab] = ode15s(@ModelPB_G_I_L_BA_RM, tspan, iv_1);
    t_stab = t;
    Ab_stab = Ab(end, :);
    t_set = t_fin;
    iv_set = Ab_stab;
    b_range = 19:30;
    tot_days = 30*365;
    Ab_days = NaN((tot_days+1), length(b_range));
    Ab_days(1, :) = Ab(end, b_range);
    t_days = 1:length(tot_days+1);
    t_days(1) = t(end) - t_fin;

    for rep = 1:tot_days
        if (rep > 1)
            initial_values = Ab_dinner(end, :)';
            initial_values(end) = initial_values(end) + dose;
            t_set = t_end;
        else
            initial_values = iv_set;
            initial_values(end) = initial_values(end) + dose;
        end

        t_add_break = 4;
        t_end = t_set + t_add_break;
        tspan = [t_set t_end];
        [t_break, Ab_break] = ode15s(@ModelPB_G_I_L_BA_RM, tspan, initial_values);
%         Ab = [Ab; Ab_break];
```

```
%       t = [t; t_break];

        initial_values = Ab_break(end, :)';
        initial_values(end) = initial_values(end) + dose;
        t_add_lunch = 8;
        t_set = t_end;
        t_end = t_set + t_add_lunch;
        tspan = [t_set t_end];
        [t_lunch, Ab_lunch] = ode15s(@ModelPB_G_I_L_BA_RM, tspan, initial_values);
%       Ab = [Ab; Ab_lunch];
%       t = [t; t_lunch];

        initial_values = Ab_lunch(end, :)';
        initial_values(end) = initial_values(end) + dose;
        t_add_dinner = 12;
        t_set = t_end;
        t_end = t_set + t_add_dinner;
        tspan = [t_set t_end];
        [t_dinner, Ab_dinner] = ode15s(@ModelPB_G_I_L_BA_RM, tspan, initial_values);
%       Ab = [Ab; Ab_dinner];
%       t = [t; t_dinner];
        Ab_days((rep+1),:) = Ab_dinner(end, b_range);
        t_days(rep+1) = t_dinner(end);

    end
    if (rp_fac == 1)
        k1 = Ab_days;
        t1 = t_days;
```

```
    elseif (rp_fac == 2)
        k2 = Ab_days;
        t2 = t_days;
    elseif (rp_fac == 3)
        k3 = Ab_days;
        t3 = t_days;
    elseif (rp_fac == 4)
        k4 = Ab_days;
        t4 = t_days;
    elseif (rp_fac == 5)
        k5 = Ab_days;
        t5 = t_days;
    elseif (rp_fac == 6)
        k6 = Ab_days;
        t6 = t_days;
    elseif (rp_fac == 7)
        k7 = Ab_days;
        t7 = t_days;
    end
end
```

Curriculum Vitae

Eric Kim

158 Otis Street Apt 2, Cambridge, MA 02141
Email: eric.kyunam.kim@gmail.com Cell: 913-742-2827

Education

Johns Hopkins University
MSE in Chemical and Biomolecular Engineering (Expected May 2020)
GPA: 4.0

BS in Chemical and Biomolecular Engineering
GPA: 3.38

Relevant Coursework

- Computational Protein Structure Prediction and Design
- Protein Engineering and Biochemistry Lab
- Advanced Topics in Pharmacokinetics/Pharmacodynamics
- Chemical & Biomolecular Engineering Lab
- Chemical & Biomolecular Engineering Product Design

Skills

- Proficient programming experience using MATLAB, Python, C++, Java, and MAPLE
- Characterization using SEM Imaging, ellipsometry, four-point probe, SDS PAGE Protocol, PCR, Column Chromatography, and CD & Fluorescence Spectroscopy
- Microsoft Excel, PowerPoint, Word
- Advanced Spanish language skills in both writing and speaking

---

Work Experience

Type 2 Diabetes Research Group, Johns Hopkins Univ. Graduate Researcher Aug 2018-Present

- Compiled and analyzed ongoing research on Type 2 Diabetes under supervision of Dr. Marc Donohue to propose an etiological mechanism of the disease.
- Completed a pharmacokinetic model in MATLAB to simulate glucose metabolism and accumulation of glycated beta amyloids in blood following high- and low-glucose meals.

Thin Films Research Group, Johns Hopkins Univ. Research Assistant Jun 2016-Sept 2017

- Operated sonicator, spin coater, hot plate, and furnace to synthesize Al doped zinc oxide thin films in a lab setting for development of a heart implant device.
- Collaborated with another lab to adjust and improve existing experimental technique for consistent high-quality thin films.
- Characterized samples using SEM imaging, ellipsometry, and four-point probe.

- Convened weekly with group and the PI, Dr. Ramsey Kraya, to discuss results of characterization of samples and adjust lab methods to achieve higher quality thin films.

Office of Institutional Research, Johns Hopkins Univ. Research Assistant Jun 2016-Sept 2017

- Assisted in compiling, analyzing, and presenting institutional data from internal and external databases under the supervision of the Vice Provost for Institutional Research.
- Attended regular meetings with project head to discuss changes and updates to projects.

Presentations

****Kim, K.E.,** Kim, D., Kraya, R. (2016, November). *Characterization of n-type ZnO thin films*. Poster presented at the 2016 INBT Undergraduate Research Symposium. Baltimore, Maryland.